Li et al. *Microsystems & Nanoengineering* (2025)11:87
https://doi.org/10.1038/s41378-025-00948-w

Microsystems & Nanoengineering
www.nature.com/micronano

REVIEW ARTICLE Open Access

PEDOT:PSS-based bioelectronics for brain monitoring and modulation

Jing Li[1,2], Daize Mo[3], Jinyuan Hu[1], Shichao Wang[1], Jun Gong[4], Yujing Huang[5], Zheng Li[6,7], Zhen Yuan[5] and Mengze Xu[1,5,6]✉

Abstract

The growing demand for advanced neural interfaces that enable precise brain monitoring and modulation has catalyzed significant research into flexible, biocompatible, and highly conductive materials. PEDOT:PSS-based bioelectronic materials exhibit high conductivity, mechanical flexibility, and biocompatibility, making them particularly suitable for integration into neural devices for brain science research. These materials facilitate high-resolution neural activity monitoring and provide precise electrical stimulation across diverse modalities. This review comprehensively examines recent advances in the development of PEDOT:PSS-based bioelectrodes for brain monitoring and modulation, with a focus on strategies to enhance their conductivity, biocompatibility, and long-term stability. Furthermore, it highlights the integration of multifunctional neural interfaces that enable synchronous stimulation-recording architectures, hybrid electro-optical stimulation modalities, and multimodal brain activity monitoring. These integrations enable fundamentally advancing the precision and clinical translatability of brain–computer interfaces. By addressing critical challenges related to efficacy, integration, safety, and clinical translation, this review identifies key opportunities for advancing next-generation neural devices. The insights presented are vital for guiding future research directions in the field and fostering the development of cutting-edge bioelectronic technologies for neuroscience and clinical applications.

Introduction

The advancement of bioelectronics has opened new frontiers in the monitoring and modulation of brain activity, providing innovative solutions for unraveling neural network dynamics and developing therapeutic interventions for neurological disorders[1]. The functionality, conformability, and biocompatibility are the main engineering considerations for the development and clinical translation of bioelectronics[2]. Particularly on the soft and highly convoluted brain surface, minimizing mechanical modulus mismatch becomes critical to achieving conformal integration of implantable electronics with neural tissue. The structure compatibility not only enhances interfacial contact to reduce electrochemical impedance and improve signal-to-noise ratio (SNR), but also mitigates shear-stress induced tissue damage during ongoing brain micromotion. Besides, engineered interfacial properties, including material chemistry to increase biocompatibility and anti-inflammatory coatings is important to reduce inflammation reaction and ensure long-term application[1,3].

As schematic illustrated in Fig. 1, Poly(3,4-ethylenedioxythiophene):polystyrenesulfonate (PEDOT:PSS) as a promising conductive polymer has gained significant attention due to its excellent combination of electrical conductivity, mechanical softness and flexibility, biocompatibility, as well as versatile processability through solution-based techniques[4,5]. These properties make PEDOT:PSS an ideal candidate for brain–computer interfaces, and other bioelectronics for both non-invasive and invasive brain monitoring and modulation. PEDOT:PSS has emerged as a versatile material for the fabrication of electrodes, sensors, and actuators that can be integrated with neural tissue[6–8]. Traditional bioelectronics, predominately fabricated from rigid inorganic

Correspondence: Mengze Xu (mengzexu@bnu.edu.cn)
[1]Faculty of Arts and Sciences, Beijing Normal University, Zhuhai 519087, China
[2]School of Systems Science, Beijing Normal University, Beijing 100875, China
Full list of author information is available at the end of the article
These authors contributed equally: Jing Li, Daize Mo, Jinyuan Hu

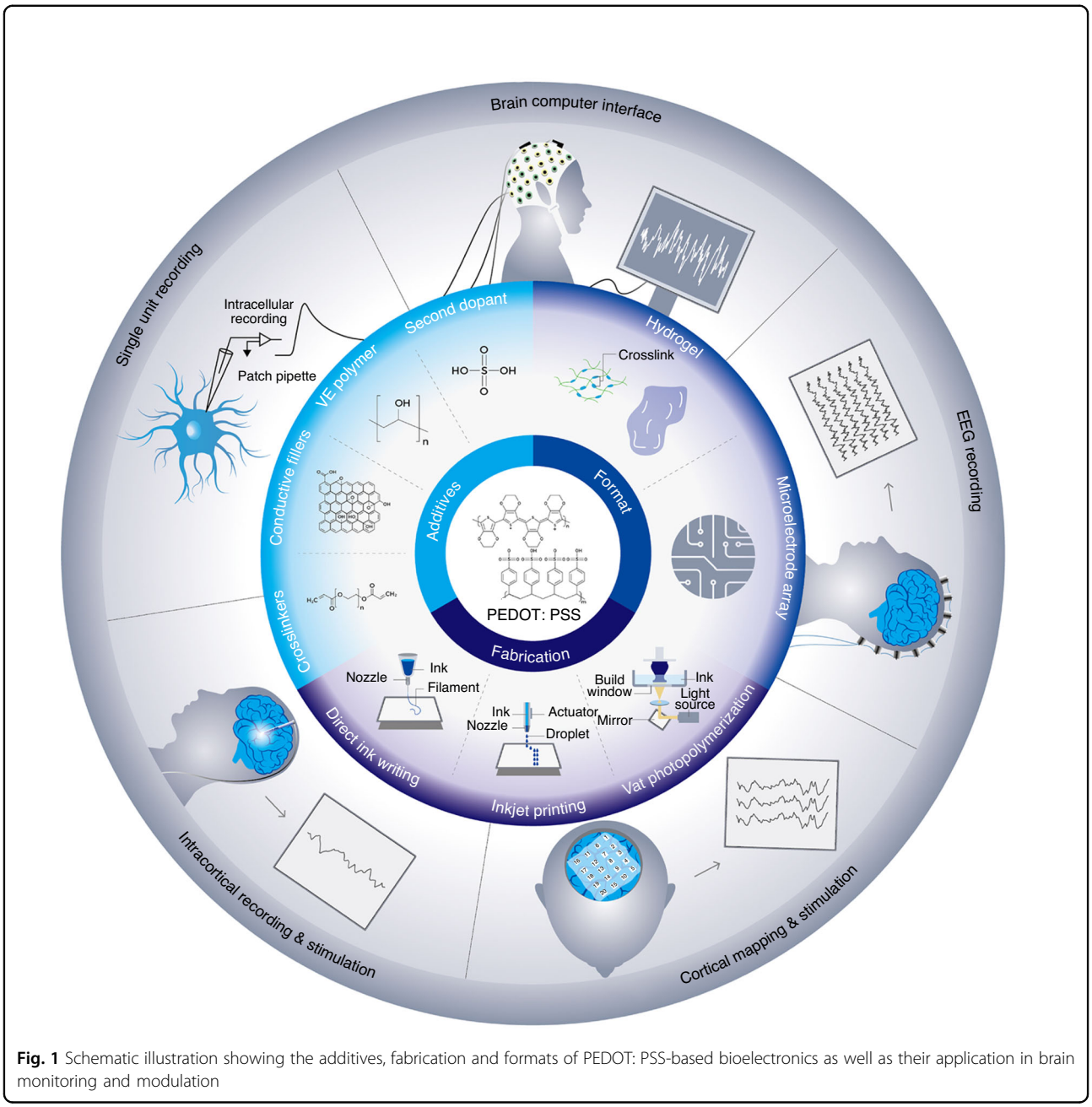

Fig. 1 Schematic illustration showing the additives, fabrication and formats of PEDOT: PSS-based bioelectronics as well as their application in brain monitoring and modulation

materials (e.g., metals, silicon) demonstrate high conductivity, but suffer from critical mechanical module mismatch (~10^6–10^8 times stiffer than brain tissue). The mechanical disparity creates disconformable interfaces, inducing tissue damage during device insertion and chronic shear-stress during physiological brain movements, which triggers neuroinflammatory response[9–11]. PEDOT:PSS-based conductive materials demonstrate superior biocompatibility and mechanical module matching (~0.1–10 MPa vs 1–4 kPa for brain tissue)[10] compared to many conventional inorganic counterparts. The intrinsic tissue-like compliance effectively suppresses foreign-body response and minimizes perturbation to neural microenvironments. In addition, PEDOT:PSS-based bioelectronics exhibit good electrochemical stability. In an experiment, it was found that a thicker PEDOT:PSS coating (in the range of 105–900 nm coating thickness) on gold electrodes can resist more electrical pulses and higher voltages without losing their charge injection capability[12]. All of these properties enable stable brain modulation in chronic practices[4]. Compared to other conductive polymers, such as polypyrrole (PPy) and polyaniline (PANI), PEDOT:PSS offers superior solution dispersibility and higher conductivity, making it an ideal

candidate for bioelectronic fabrication[13]. Additionally, various additives can be incorporated into PEDOT:PSS-based composites to further enhance the conductive and mechanical performance. Owing to these merits, PEDOT:PSS-based conductive biomaterials have been widely utilized in bioelectronics, either as hydrogels or thin films deposited on substrates, and we have summarized them in Table 1.

PEDOT:PSS's versatility is further enhanced by its adaptability to various fabrication techniques, including 3D printing and 2D modification technologies, making it a highly scalable option for bioelectronics. 3D printing technology enables the precision fabrication of customized architectures and integrated electronic components. Especially, 3D technologies provide feasible and controllable processes for printing PEDOT: PSS-based hydrogels as bioelectronic interfaces. The hydrogel-based ultrasoft bioelectronics (kPa scale) have a similar mechanical modulus to brain tissue, making them a promising candidate for long-term brain modulation with reduced inflammatory responses. In contrast, conventional 2D fabrication methods (e.g., spin coating, electrochemical deposition, and photolithography)[14] dominate applications requiring nanoscale-to-micron resolution[15,16]. This level of precision is critical for the fabrication of fine features, such as microelectrodes, electrode arrays, and intricate patterns that are required for bioelectronic devices like neural interfaces or biosensors.

Brain monitoring and modulation is an important subject in brain science research, which is necessary to explore the mechanisms of how brain controls feeling, behavior, and cognition. Brain monitoring and modulation studies provide different kinds of paradigms (invasive, semi-invasive, and non-invasive ways) to reveal the correlation between the brain structures and functions at the cell, tissue, and system levels[17]. Besides, brain neural activity monitoring and modulation is an efficient medical approach for the diagnosis and treatment of a series of brain disorders, including epilepsy, Parkinson's disease, Alzheimer's disease, sleep disorders, and major depression. Critically, the emergence of chronic closed-loop deep brain modulation systems has revolutionized therapeutic precision by enabling real-time detection of pathological biomarkers (e.g., amygdala gamma power) followed by adaptive neurostimulation, resulting in sustained improvement in depression[18]. Moreover, in the cutting-edge area of brain–computer interface, brain monitoring and modulating technologies are critical to achieving high neural signal detection and real-time translation[19].

Electrodes, as the connective channels between the brain and external electrical devices, are the critical tools for recording and modulating neural activity. The surface property of electrodes often determines the quality of the acquired neural signal. For example, low surface impedance electrodes are often preferred as they enable relatively high-SNR neural signal acquisition. In addition, a conformal contact between the skin and electrodes is important to maintain stable signal acquisition[20,21]. Developing flexible, comfortable, stable, high charge injection capacity (CIC), high spatial-temporal resolution neural electrodes is necessary for achieving precise and robust neural stimulation as well as for acquiring accurate and reliable neural signal[22].

Considering the rapid development of PEDOT:PSS and neuroscience research, as well as the tremendous potential for the application of PEDOT:PSS-based bioelectronics in neuroscience studies, this review explores the cutting-edge developments in PEDOT:PSS-based organic bioelectronics for brain neural monitoring and modulating. We focus on advancements in material properties, fabrication strategies, and their integration into neural devices. In the end, we provide the outlook for the future opportunities and challenges, such as the development of multifunctional bioelectrodes and environment-responsive bioelectronics, the application of advanced 3D/4D/5D printing technology for interface fabrication, as well as the clinical considerations.

PEDOT:PSS-based conductive biomaterials

PEDOT:PSS's structure, comprising positively charged PEDOT chains complexed with negatively charged PSS chains, imparts unique properties, including solution processability and high electronic/ionic conductivity. PEDOT:PSS is a polyelectrolyte complex consisting of two constituents. Among the complex, PEDOT is the conductive component with positive charges, formed by the polymerization of 3,4-ethylenedioxythiophene (EDOT) monomer, where the sulfur atoms in the two ethylenedioxy groups attached at the 3 and 4 positions of the ring ensure electronic conductivity by π-electron delocalization along the polymer backbone[23,24]. PSS is an insulating polymer carrying negative charges derived from polystyrene with the functionalization of sulfonate group ($-SO_3H$)[25]. Due to the inherent hydrophobicity of PEDOT in aqueous environments, PSS can electrostatically adsorb onto the PEDOT surface through Coulombic interactions, effectively stabilizing the insoluble polymer into a water-dispersible colloidal system when the generally accepted complex structure model is the small segments of PEDOT in close contact with the PSS bundles[23]. In water dispersion, PEDOT chains aggregate due to π-π interactions and Van der Waals forces and the formed crystalline domains provide pathways for electrical conduction when the PSS matrix takes up solvated ions and water to induce ionic transport and enhance the water solubility and dispersibility of the complex, enabling the diverse 2D/3D solvent processing techniques, such as direct ink writing, inkjet printing, and spin coating[26,27].

Table 1 The summary of PEDOT: PSS-based neural interfaces for brain recording and modulation

Application category	Active components	Format	Printing method	Postprocessing method	Electrical properties	Mechanical properties	Resolution (μm)	SNR (dB)	Ref.
Single-unit recording	PEDOT:PSS, DMSO	Hydrogel	3D printing	Dry annealing	Conductivity: 28 S/cm (annealed state)	Young's modulus: 1.1 MPas (annealed state)	/	/	14
	PEDOT:PSS	MEA	ECD	/	Electrical impedance: ~52 kΩ at 1 kHz		/	~4	151
	PEDOT:PSS, CNT, PHEMA	Spherical	ECD	/	Electrical impedence: ~1 kΩ at 1 kHz	Young's modulus: 10 kPa	100	~1.7	198
	PEDOT:PSS	Free-floating	ECD	/	Electrode impendence: 133 kΩ at 1 kHz	/	/	22–24	199
	PEDOT:PSS, DA	Hydrogel	Crosslinking	Photocuring	Conductivity: 4176 S/cm (annealed)	/	15.5	/	152
Intracortical recording	PEDOT:PSS, DMSO	MEA	Material extrusion	Dry annealing	Conductivity: 137 S/cm (ink)	/	/		200
	PEDOT:PSS, GO	MEA	ECD	/	Electrical impedance: 10.5 kΩ at 1 kHz	/	/	/	157
	PEDOT:PSS, MWCNT	MEA	ECD	/	Electrical impedance: 23 kΩ at 1 kHz	/	/	/	158
	PEDOT:PSS, PVA	Hydrogel	Crosslinking	Photocuring	Electrical impedance: 1.14 kΩ at 1 kHz	Stretch: 72% strain Young's modulus: 191 kPa	/	~3–6	155
	PEDOT:PSS, Pt NPs, short MWCNT	MEA	ECD	/	Electrical impedance: 12 kΩ at 1 kHz	/	/	/	201
	PEDOT:PSS, Pt NPs	MEA	ECD	/	Electrode impedance: 3.4 kΩ at 1 kHz	/	/		154
	PEDOT:PSS, Pt NPs	MEA	ECD	/	Electrode impedance: 17.2 kΩ at 1 kHz	/	/	~17	202
	PEDOT:PSS	MEA	ECD	/	Electrode impedance: 76 kΩ at 1 kHz	/	/	/	203
	PEDOT:PSS	MEA	ECD	/	Electrode impedance: 1 kΩ at 1 kHz	/	/	~6–12	138

Table 1 continued

Application category	Active components	Format	Printing method	Postprocessing method	Electrical properties	Mechanical properties	Resolution (μm)	SNR (dB)	Ref.
	PEDOT:PSS, Pt NPs, MWCNT	MEA	ECD	/	Electrical impedance: 32.46 kΩ at 1 kHz	/	/	/	159
	PEDOT:PSS, SWCNT	MEA	ECD	/	Electrical impedance: 16 kΩ at 1 kHz	/	/	>3	204
	PEDOT:PSS	Monolayer open-mesh	Spin coating	Thermal annealing	/	/	/		205
Intracortical recording & stimulation	PEDOT:PSS, IrOx	MEA	ECD	/	Electrical impedance: 42 kΩ at 1 kHz CSC: 25 mC/cm^2	Bending modulus: 4×10^{-13} $N{\cdot}m^2$	/	~8–16	206
	PEDOT:PSS, PHEMA	MEA	ECD	/	CICmax: 3.31 mC/cm^2	Young's modulus: 322 kPa			165
	PEDOT:PSS, H_2SO_4	Film	Spin coating	Thermal annealing	Conductivity: 652 S/cm Electrode impedance: 90 kΩ at 1 kHz	/	/	/	166
	PEDOT:PSS	Microprobe	ECD	/	/	/	/	/	167
Cortical mapping	PEDOT:PSS, EG, DBSA, GOPTS	MEA	Spin coating	Thermal annealing	Electrode impedance: 12–13 kΩ at 1 kHz		50		171
	PEDOT:PSS, PAM	Hydrogel	Crosslinking	/	/	Elastic modulus: 2 kPa	/		207
	PEDOT:PSS, EG	MEA	Spin coating	Thermal annealing	Electrode impedance: 25.8 kΩ at 1 kHz	/	/		173
	PEDOT:PSS, glycerol, DBSA	MEA	Spin coating	Thermal annealing	Electrode impedance: 3.5 kΩ at 1 kHz	/	/		7
	PEDOT:PSS, DBSA	Hydrogel	DIW	Thermal annealing	Conductivity: 35 S/cm (hydrogel); 600 S/cm (dry-annealed state)	Young's modulus: 31 kPa (hydrogel) 1.5 MPa (dry-annealed state)	10		177
	PEDOT:PSS, MWCNT	MEA	ECD	/	Electrical impedance: 20 kΩ at 1 kHz		60	/	172
	PEDOT:PSS	MEA	ECD	/	Electrical impedance: 2 kΩ at 1 kHz	/	/	/	135
	PEDOT:PSS	MEA	ECD	/	/	/	/	~2–12	208

Table 1 continued

Application category	Active components	Format	Printing method	Postprocessing method	Electrical properties	Mechanical properties	Resolution (μm)	SNR (dB)	Ref.
	PEDOT:PSS-b-PPEGMEMA	Block-brush film	Crosslinking	/	Volumetric capacitance: 120 F/cm^3	Young's modulus: 1.7 MPa	/		174
	PEDOT:PSS, GOPS, EG, DBSA	MEA	Spin coating	Thermal annealing	Electrical impedance: 147 kΩ at 1 kHz	/	/	/	209
	PEDOT:PSS, EMIM:TCB	Hydrogel	DIW	/	Conductivity: 286 S/cm	Storage modulus: 105 kPa Yield stress: 104 kPa	50		45
Cortical mapping & stimulation	PEDOT:PSS, silk fibroin, PEGDA	Hydrogel	Crosslinking	/	Sheet resistance: 160 Ω /sq	Stretch: 200% strain	25		178
	PEDOT:PSS, EG	MEA	Spin coating	Thermal annealing	Electrical impedance: 55 kΩ at 1 kHz CIC: 0.7 mc/cm^2	/	/	/	179
	PEDOT:PSS, AV gel, glycerol, DMSO	Hydrogel	Crosslinking	Thermal annealing	Maximum transconductance: 250 mS	Young's modulus: 154 MPa	/		175
EEG	PEDOT:PSS	Fiber	Screen printing	/	Sheet resistance: 67 Ω/sq	/	/		210
	PEDOT:PSS, d-sorbitol	Fiber	Material extrusion	/	Double-layer capacitance: 2.72 μF	/	10.7		211
	PEDOT:PSS, GO, SDS, BSL	Film	Spin coating	Thermal annealing	Conductivity: 4142 S/cm	Young's modulus: 640 kPa	/	~23	112
	PEDOT:PSS, SDS, GO	Film	Spin coating	Thermal annealing	Sheet resistance: 20.8 Ω /sq Conductivity: 3727 S/cm	/	/		184
BCI	PEDOT:PSS, PVA, borax	Hydrogel	Material extrusion	/	Conductivity: 2.3×10^{-3} S/cm Impedance: 10 kΩ at 0.1 Hz	Young's modulus: 2.5 MPa	/	13–15	109
	PEDOT:PSS, SA, PAM, glycerol, KCl	Hydrogel	Crosslinking	Photocuring	Impedance: <5 kΩ at 0.5–50 Hz	/	/	/	189

The charge transport efficiency in PEDOT:PSS systems is fundamentally constrained by their inherent morphological characteristics. In pristine PEDOT:PSS, the amorphous arrangement creates topological disorder through random chain orientations and insufficient π-π stacking. This structural discontinuity establishes multiple charge trapping sites, significantly impeding long-range carrier mobility[24,28]. Furthermore, in pristine PEDOT:PSS, the concentrations of charge carriers—polaron ($PEDOT^{+}$) and bipolaron ($PEDOT^{2+}$) are low and their distribution is localized. These limitations result in a conductivity of less than 1.0 S/cm[29]. Beyond conductivity, pristine PEDOT:PSS also has a low solid content (1.0–1.3%), making it too diluted for efficient solvent processing using the aforementioned techniques[30]. Moreover, there is an inherent trade-off between conductivity, mechanical flexibility, and stability in pure PEDOT:PSS. While a highly ordered and strong stacking PEDOT matrix increases conductivity, it also increases modulus and rigidity[31]. Pure PEDOT:PSS exhibits limited flexibility with a relatively high Young's modulus (1–2 GPa), and poor stretchability with an elastic strain of only 2% due to the rigid and brittle PEDOT-rich domain. These mechanical constraints hinder its long-term applications in contact with brain tissue[32]. These drawbacks have spurred research into additive strategies to optimize the electrical, rheological, and mechanical performance. The commonly employed additives include second dopants, viscoelastic polymers, and conductive fillers (Fig. 2). Second dopants are the most widely used fillers that can significantly enhance conductivity; however, they often exhibit a certain level of toxicity and are not easily removable. Viscoelastic polymers can improve the viscoelasticity and rheological properties of PEDOT:PSS, but their insulating nature may lead to a decrease in conductivity. Conductive fillers can enhance both conductivity and mechanical properties, yet they come at a higher cost and pose a risk of aggregation. Crosslinkers can improve mechanical performance but may reduce conductivity and generally require laser-induced crosslinking.

Second dopants

In pristine PEDOT:PSS, the excessive insulating PSS chains cause a discontinuous conducting pathway in PEDOT, thus limiting charge transport[33,34]. Second dopants can modify the primary PSS-doped PEDOT by weakening the Columbic interactions between PEDOT+ and PSS-, inducing phase separation between PEDOT and PSS chains. This process alters the PEDOT conformation, leading to the formation of PEDOT-rich domains with enhanced crystallinity and crystal ordering, which facilitates the transport of polarons or bipolarons, thereby improving electrical conductivity[33–35]. Macroscopically, phase separation and conformation rearrangement also increase the colloidal density of PEDOT, resulting in higher viscosity and making the material more suitable for 3D printing[4]. Beyond promoting PEDOT-PSS separation, second dopants can significantly expand the free volume within PEDOT:PSS polymer chains, enhancing flexibility and stretchability[31]. The most well-studied second dopants for PEDOT:PSS include polar solvents, ionic liquids, deep eutectic solvents, surfactants, and strong acids. Polar solvents promote the rearrangement of PEDOT chains, which enhances charge transport, and they are generally low-cost and easy to integrate into solution processes. However, their rapid evaporation can affect film uniformity if not carefully controlled, and they may not achieve the same level of conductivity enhancement as ionic liquids or strong acids. Ionic liquids, on the other hand, can improve both the electronic properties and the flexibility of PEDOT:PSS, often resulting in high conductivity. Their main drawbacks are higher cost and potential biocompatibility issues due to residual ionic liquid, which can be a concern in sensitive bioelectronic applications. Deep eutectic solvents offer a greener alternative, as they are typically composed of benign, low-cost ingredients. Although they improve processability and film formation, their enhancement of electrical properties is generally less dramatic compared to ionic liquids. Surfactants lower surface tension, enabling more homogeneous coatings and better interface contact with substrates. Despite this advantage, they do not significantly boost conductivity and, in some cases, excessive surfactant content may even hinder electrical performance. Strong acid treatments can effectively remove excess insulating PSS, leading to a highly conductive, PEDOT-rich film with substantial conductivity improvements. However, the harsh conditions associated with strong acids can damage flexible substrates or delicate biointerfaces, and residual acidity may render them unsuitable for certain bioelectronic applications.

Polar solvents

Polar solvents with a high boiling point are well-investigated second dopants for increasing the conductivity of PEDOT:PSS. When these solvents are added, the polar groups form hydrogen bonds with the sulfonic acid groups of PSS. This interaction triggers the dissolution and partial diffusion of PSS away from PEDOT, along with structural rearrangement, thereby improving conductivity[31]. Among these solvents, dimethyl sulfoxide (DMSO) is the most commonly used to boost the performance of PEDOT: PSS-based conductive materials. In one experiment, enhanced structural order and π-stacking intensity were observed after DMSO treatment, as monitored by wide-angle grazing incidence scattering[36]. To compare the performance of various polar solvents, a

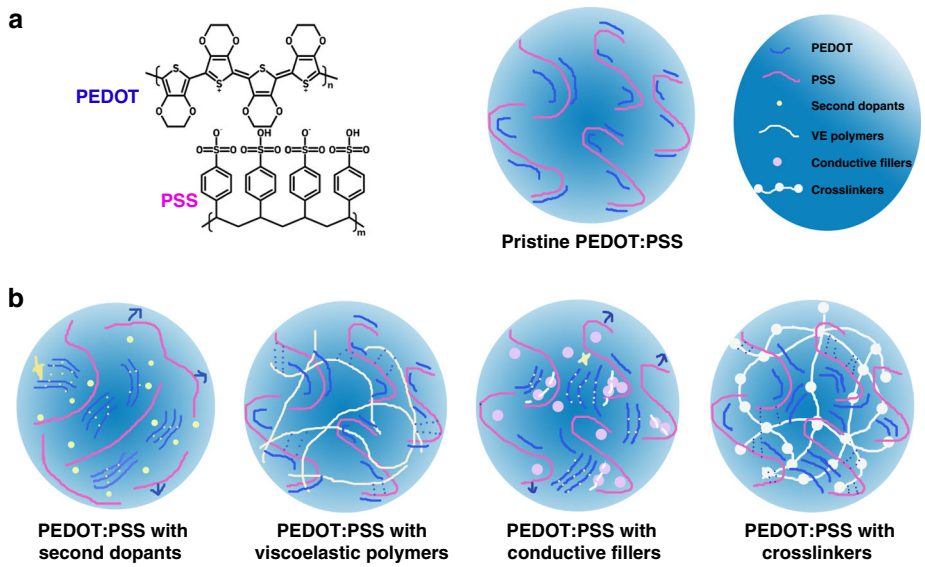

Fig. 2 Graphic illustration of PEDOT: PSS-based conductive materials. a Schematic illustration of PEDOT:PSS. Left: molecular structure; Right: PEDOT:PSS in aqueous phase. **b** Schematic illustration of PEDOT:PSS with different additives in aqueous phase. Second dopants facilitate the PSS chain separation from the PEDOT:PSS complex (blue arrow) by charge screening effect. The phase separation enables PEDOT chain arrangement and the formation of π stacking (yellow dashed line), which improves the electrical transduction (yellow star). Viscoelastic polymers form hydrogen bond with PSS chain (blue dashed line), making the complex system more viscous and stretchable. Conductive fillers enhance the charge transport (white dashed line). Simultaneously, the fillers promote PSS removal (blue arrow) and PEDOT chain arrangement (yellow dashed line), all of which enhance the conductivity (yellow star). Crosslinkers form a long interconnected network with PEDOT:PSS systems by hydrogen bond with PSS (blue dashed line)

surfactant-free PEDOT:PSS dispersion was individually mixed with 5 wt% of ethylene glycol (EG), DMSO, *N*, *N*-dimethylformamide (DMF), or glycerol for inkjet printing. The resulting printed objects exhibited sheet resistance values of approximately 335, 767, 1914, 2371 Ω/sq for the EG, DMSO, DMF, and glycerol inks, respectively, while pure PEDOT:PSS ink showed a sheet resistance of around 6.2 kΩ/sq. This clearly demonstrates that polar solvents can effectively reduce resistance and enhance conductivity[33]. Additionally, other glycol-based additives—such as diethylene glycol, triethylene glycol, hexaethylene glycol, and ethylene glycol monomethyl ether also exhibited improvement in conductivity[37]. Beyond this, solvents like sorbitol[38], methanol[39], and acetone[40] have demonstrated the capability to increase both crystallization and conductivity of PEDOT:PSS.

Ionic liquids

Ionic liquids (ILs) are organic salts that remain liquid at ambient conditions, eliminating the need for dissolution in another solvent. Their bulky and asymmetric organic anions and cations hinder the lattice formation[41,42]. Based on the hard-soft-acid-base principle, ILs with hydrophilic hard cations and hydrophobic soft anions can decouple the hydrophilic PSS- from the hydrophobic PEDOT +, promoting the growth of conductive PEDOT+ domains. The low binding energy between the cations and anions enables an ion exchange with PEDOT:PSS, as shown in the equation:

$$\mathrm{PEDOT:PSS} + \mathrm{Cation:Anion} \leftrightarrow \mathrm{PEDOT:Anion} + \mathrm{PSS:Cation}$$

The strong counterion exchange not only facilitates the separation of PEDOT and PSS but also enhances the hydrogen bonding between colloidal particles, leading to improved PEDOT chain arrangement, increased crystallinity, and the formation of band-like carrier transport pathways. These effects are critical for improving both the rheological properties and electrical conductivity of PEDOT:PSS[29,43]. Meanwhile, the ILs can increase the free volume within the material, making PEDOT:PSS more stretchable[31]. For example, Vivian et al. demonstrated that the ionic liquid, (3-butyl-1-imidazolio)-1-butanesulfonic acid triflate (BIM-Tf), can screen the electrostatic repulsion between the PEDOT:PSS microgels, promoting the formation of a connected macroscopic network and increasing gel strength, as indicated by the storage modulus (G'), with rising ionic strength[44]. Another commonly used ionic liquid is 1-ethyl-3-methylimidazolium (EMIM): tetracyanoborate (TCB), which induces PEDOT:PSS gelation[45]. Moreover, studies have shown that protic but

not acidic ILs, *N*-propyl pyrrolidinium (PYR3):TCB and *N*-ethylimidazolium (EIM):TCB outperform EMIM:TCB in enhancing PEDOT domain size, order, and p-doping level[46]. Additional additives like lithium bis (trifloromethanesulfonyl) imide (Li-TFSI)[47], Cobalt (II) chloride hexahydrate ($CoCl_2{\cdot}6H_2O$-ChCl)[48] have also been found to improve the crystalline conformation and transduced conductivity of PEDOT:PSS. However, the toxicity of most ILs, which can lead to cell damage, limits their applications in bioelectronic interfaces. In contrast, tris(2-hydroxyethyl)-methylammonium methylsulfate ([MTEOA][$MeOSO_3$]), a third-generation IL, is favored for its low environmental toxicity, good biocompatibility, and biodegradability[49]. It has been shown to enhance the PEDOT chain ordering, achieving a conductivity of 625 S/cm, while not causing statistically significant cell death, detachment, or containment on human dermal fibroblasts, human keratinocytes, human epidermal keratinocytes, and human colon mucosal epithelial over a 2-day testing period[50].

Deep eutectic solvents

Deep eutectic solvents (DES) are low-melting mixtures formed by combining two or more components in a specific molar ratio. DES exhibits melting points lower than those of their individual components, primarily due to the formation of an extensive hydrogen bonding network[41,51]. The cation species in DES can interact with PSS-, thereby weakening the Coulombic interactions between PEDOT and PSS and promoting increased PEDOT crystallinity. And the intermolecular hydrogen bonds between DES and PEDOT:PSS facilitate improved PEDOT chain alignment and network formation, leading to more efficient charge transport and enhanced mechanical stability. Moreover, the highly polarizable anionic and cationic species in DES have been reported to enhance the ionic conductivity within the PEDOT:PSS blend[52,53]. Compared to traditional organic polar solvents such as DMSO and ILs, DESs are more environmentally-friendly, cost-effective, easier to prepare, and exhibit higher biodegradability and biocompatibility[54]. Leveraging these advantages, choline chloride: lactic acid (ChCl:LAC) was incorporated into photoactive PEDOT:PSS-poly(ethylene glycol) diacrylate (PEGDA) inks, resulting in up to a ninefold improvement in electronic conductivity (~26–36 S/cm) compared with PEDOT:PSS-PEGDA alone. This enhancement was accompanied by increased intermolecular interactions, as evidenced by higher storage and loss moduli. Furthermore, the resulting composite material demonstrated good biocompatibility, as it did not induce significant cell death in two fibroblast cell lines over a 24-h culture period[55]. Owing to the dual electronic and ionic conductivity and extensive hydrogen bonding interactions in DES-doped PEDOT:PSS, Li et al. developed an interpenetrating network comprising PEDOT:PSS, gelatin and a DES composed of glycerol and choline chloride in a 1:1 ratio. This composite achieved an impressive modulus of approximately 0.3–1.1 MPa and exhibited high conductivity along with an SNR of 30–40 dB[56].

Surfactants

Surfactants enhance the conductivity, mechanical properties, and wettability of PEDOT:PSS through several mechanisms. First, they disrupt the interactions between PEDOT and PSS, thereby improving the π−π stacking of PEDOT chains and facilitating the removal of PSS. Second, Second, by increasing the free volume between polymer chains, surfactants enhance the stretchability of the material. Third, they improved the wettability of PEDOT:PSS on hydrophobic substrates e.g., polydimethylsiloxane (PDMS), leading to more uniform dispersion, stronger adhesion, and smoother films[57–59]. For example, fluorosurfactant Zonyl exhibits a synergistic effect with DMSO by not only enhancing the conductivity of PEDOT:PSS but also improving its wettability. This enables the facile deposition of conductive films on PDMS, resulting in stretchable and flexible electrodes[60]. Other non-ionic surfactants, such as 4-dodecylbenzenesulfonic acid (DBSA)[61], polyoxyethylene octyl phenyl ether (Triton X-100)[62], Tween 80[63]-have also been shown to positively impact the mechanical stability, conductivity, and film processing characteristics of PEDOT:PSS. Ionic surfactants tend to be more effective than non-ionic ones because their ionic units can interact more strongly with the charged species in PEDOT:PSS through electrostatic interactions[31]. In a study by Chen et al., both cationic surfactants (butyl trimethyl ammonium bromide, hexyltrimethylammonium bromide, and *N*-octyltrimethylammonium bromide) and anionic surfactants (sodium octyl sulfate, and sodium dodecyl sulfate) promoted phase separation by interacting with PSS- or PEDOT+, and they increased the free volume for the motion of the polymer chains by introducing soft alkyl segments. Notably, cationic surfactants exhibited a stronger effect on enhancing the stretchability of PEDOT:PSS, as they could break the hydrogen bonds among PSS chains and further increase segmental mobility—an effect not observed with anionic surfactants[58].

Acids

Strong acid treatment can induce proton transfer from the acids to the PSS groups in PEDOT:PSS, promoting phase separation that increases solid content, elongates the conjugated PEDOT chain length, and enhancesπ−π stacking, resulting in enhanced conductivity and mechanical stability[64,65]. To investigate the effects of acid properties on the conductivity of PEDOT:PSS, researchers added various mineral acids—sulfuric acid (H_2SO_4), perchloric

acid ($HClO_4$), phosphorousacid (H_3PO_3), pyrophosphoric acid ($H_4P_2O_7$), phosphoric acid (H_3PO_4), nitric acid (HNO_3), hexafluorophosphoric acid (HPF_6), hydrochloric acid (HCl), and sulfurous acid (H_2SO_3)—at different concentrations to pristine PEDOT:PSS. The results indicated that acids with high boiling point (Tb >150 °C) and low acid dissociation (pKa<3) were prerequisites for conductivity enhancement. Moreover, the softness parameter of the acid anion played a critical role: anions with lower softness parameters, due to their higher polarizability, form stronger interactions with $PEDOT^+$, leading to more efficient doping. Since H_2SO_4 met these criteria, 0.08 M H_2SO_4-doped PEDOT:PSS achieved the highest conductivity of 2244S/cm[66]. Although strong acids can significantly enhance the conductivity, their interaction with plastic substrates can compromise the stability of bioelectronic devices. To address issues related to corrosion and residual acid, milder treatments using methanesulfonic acid (CH_4SO_3) or H_3PO_4 have been employed, achieving conductivity enhancements comparable to H_2SO_4 while offering better stability on plastic substrates.

Viscoelastic polymers

Viscoelastic polymers exhibit both viscous and elastic properties when deformed. These polymers can enhance the mechanical flexibility and stretchability of PEDOT:PSS films by absorbing and dissipating mechanical stress, imparting mechanical properties similar to their own. It should also be noted that the introduction of viscoelastic polymers can enhance the durability and mechanical stability of the conductive network in PEDOT:PSS. They can lower the probability of cracking or damage that might occur to the conductive network when PEDOT:PSS is used in various situations, therefore expanding its range of applications[67]. In addition, these polymers have a significant impact on the processing characteristics of PEDOT:PSS. They increase the solution's viscosity and impart desirable rheological properties, such as shear-thinning behavior. This means that when shear force is applied, the solution becomes less viscous, making it easier to handle during processes like coating, printing, or spraying. This improvement simplifies solvent-based processing techniques and can lead to more consistent and high-quality film formation[4,31]. A variety of polymers -such as polyethylene glycol (PEG)[68], poly (vinyl alcohol) (PVA)[68–72], poly (ε-caprolactone) (PCL)[73], poly (lactic acid) (PLA)[74], polyurethane (PU)[75,76], and polyethylene oxide (PEO)[77,78]—have been employed to enhance the elasticity and rheological properties of PEDOT:PSS-based systems. For example, a stretchable material fabricated by incorporating PEG and PU into PEDOT:PSS exhibited high elongation at break (350%), high toughness (24.6 MJ/m^3), moderate conductivity (10 S/cm) as well as excellent recyclability with no significant loss in mechanical properties and conductivity after 20 cycles of use. The improvement in mechanical stability is primarily attributed to the optimized composite design. This mechanical stability arises from the composite design: the soft segments of PU improved the self-healing and recyclability, and its hard segments enhanced the strength and durability. PEG interacted with both PU and PEDOT:PSS via hydrogen bonding, promoting flexible chain mobility and energy dissipation under stress[79]. However, most viscoelastic polymers are insulating, potentially reducing PEDOT:PSS conductivity. The balance between conductivity and mechanical as well as rheological properties can be regulated by tuning the PEDOT:PSS-to-polymer ratio[31]. Exceptions like PEO can enhance conductivity as well as mechanical and rheological properties at the same time. Under nitrogen protection and heat treatment, PEO interacts with PSS^-, prompting the partial release of PEDOT from the complex. The liberated PEDOT chains then entangle to form interconnected networks, which enhance electrical transport while preserving the viscoelastic property of the composite. However, despite these advantages, the required thermal processing under nitrogen conflicts with scalable manufacturing protocol, and prolonged heating may degrade the long-term performance of PEDOT:PSS, which restricts PEO's widespread application[33,80,81]. In a study by Plog et al., various viscoelastic polymers-including PEO, poly(*N*-isopropylacrylamide) (PNIPAM) and polyacrylamide (PAM)-were evaluated for their effects on the electrical conductivity and rheological behavior of PEDOT:PSS dispersions. All three polymers induced shear-thinning behavior (where viscosity decreased), a crucial attribute for many liquid processing techniques that require high viscosity at low shear rates (1/s). However, only 52 wt% PEO achieved an electrical conductivity more than 15 times higher than that of pristine PEDOT:PSS[82]. Similarly, carboxymethylated cellulose improves both the conductivity and stretchability of PEDOT: PSS-based bioelectronics. The hydroxyl groups in cellulose interact with the sulfonate groups on PSS, promoting phase separation between PEDOT and PSS, and facilitating the formation of a more interconnected, conductive network with enhanced resistance to mechanical stress. Moreover, as a natural polymer, cellulose is inherently more biocompatible and biodegradable than many synthetic polymers[83–85].

Conductive fillers

Conductive fillers offer satisfying conductivity and can further enhance the electrical performance of PEDOT:PSS. Their interaction with PEDOT:PSS creates an interconnected network that not only improves electron transport but also enhances the rheological properties and mechanical stability of the final product[86,87]. Conventional conductive fillers include metal salts, metal-based nanostructures, and carbon-based nanostructures. For

instance, Wang et al. found that a series of metal halides ($InCl_3$, $CuCl_2$, $NiCl_2$, $MgCl_2$, LiCl, and NaCl) can efficiently improve both conductivity and elongation ability. This improvement was attributed to the strong interaction between metal halides and PSS-, which resulted in the removal of PSS and the accumulation of PEDOT[88]. Additionally, the hydrophilic 2D transition metal carbide, Ti_3C_2 Mxene nanosheet, has been reported to enhance the rheological properties and conductivity of PEDOT:PSS. Inks incorporating MXene exhibit distinct shear-thinning properties and a yield stress up to 398 Pa, making them ideal for extrusion-based printing. Meanwhile, hydrogels printed from these inks achieved high conductivity of ~1525.8 S/m at low solid concentration (≥wt%), due to the phase transition and redispersion of PEDOT:PSS induced by the Mxene interaction[89]. Other metallic-based nanostructures, such as gold nanoparticles (Au NPs)[90], silver nanowires (Ag NWs)[91], and molybdenum disulfide (MoS_2)[92], have also been incorporated into PEDOT:PSS-based materials. In contrast, carbon-based nanocomposites are low-cost, environmentally-friendly and easily functionalized[93]. These carbon-based fillers enhance conductivity by inducing PEDOT separation through a charge screening effect and promoting PEDOT chain rearrangement. Various carbon-based materials, including 0D carbon dots[94], 1D carbon nanotubes[95], 2D materials such as graphene, graphene oxide (GO)[96], and reduced graphene oxide (rGO)[97], have been investigated to improve both the conductive and mechanical properties of PEDOT:PSS.

Crosslinkers

Crosslinkers are agents which connect two polymers through physical or chemical interactions, altering the molecular arrangement to enhance mechanical properties, rheological properties and conductivity. Physical crosslinking methods for PEDOT:PSS include ionic bonding, hydrogen bonding, π–π stacking, and metal coordination[98]. For instance, sodium trimetaphosphate (STMP) serves as an ionically conducting inorganic binder that improves both the conductivity and mechanical strength of conductive materials[99]. When incorporated into PEDOT:PSS hydrogels, STMP induces sufficient physical crosslinking to improve the hydrogel conductivity, wettability, and rheological properties[100]. Similarly, Mydhili et al. developed a composite of PEDOT:PSS, PVA, and GO that exhibited enhanced conductivity. This improvement was attributed to the strong π–π interaction between GO and PEDOT:PSS, as well as hydrogen bonding between PVA and PEDOT:PSS[101]. In addition to these approaches, second dopants, strong acid treatments, viscoelastic polymers, and conductive fillers also enhance the conductive and mechanical performance of PEDOT:PSS inks by physical crosslinking.

Chemical crosslinking in PEDOT:PSS systems is typically achieved through the formation of covalent bonds, with radical polymerization being one of the most widely applied strategies. In radical polymerization, monomers polymerize in the presence of initiators, commonly photoinitiators that generate reactive species under light irradiation. These reactive species attack or modify the functional groups on the monomers to initiate a chain reaction. Different photoinitiators induce the photopolymerization via distinct mechanisms. The free radical photoinitiators, such as derivatives of benzoin, acetophenone, hydroxyalkylphenones, and acylphosphine, generate free radicals upon light irradiation that attack the double bonds in monomers, like acrylate and methacrylate derivatives. In contrast, cationic photoinitiators such as aryl iodonium salts and sulfonium derivatives produce acids when exposed to light, which react with vinyl ethers and epoxy resins to induce chain extension[102–104]. The polymerization process yields interconnected polymer networks that physically trap the PEDOT:PSS, thereby enhancing the composite's structural integrity. Materials such as PEG diacrylate (PEGDA)[105], PEG dimethacrylate (PEGDMA)[106], gelatin methacrylate[107], and polymethyl methacrylate (PMMA)[108] have exhibited good gel formation ability and have been widely applied in PEDOT:PSS-based inks. In one study, PEDOT:PSS, PEGDA was mixed with PEGDA of various molecular weights ($M_n = 250, 575, 700\,Da$) and photoinitiators to produce photocurable inks. These inks were processed using 3D digital light printing to form flexible, shape-defined hydrogels. The resulting crosslinked hydrogels exhibited soft mechanical properties, with a Young's modulus of ~3 MPa-comparable to human skin tissue. And because the hydrogels were formed by free radical species-induced crosslinking at the end of PEGDA chains, lower molecular weight (shorter chain length) PEGDA resulted in a higher cross-link density and smaller mesh size. The reduced mesh size limited the hydrogel's swelling and concentrated the PEDOT within the network, thus increasing the conductivity[105]. Chemical crosslinking can also be induced through reactions between small molecules and the functional groups of polymers. For example, adding borax into the PEDOT:PSS/PVA hydrogels induced reversible borax/hydroxyl bonds between borax and PVA matrix, along with hydrogen bonds between PSS and either PVA or borax. These interactions significantly improved the mechanical integrity and electrical-healing ability of the hydrogel after mechanical damages[109].

Intensive studies have demonstrated that the combination of multiple additives, rather than a single additive,

can synergistically enhance the conductivity, stretchability, and flexibility of PEDOT:PSS-based bioelectronics. For instance, a conductive hydrogel was developed using PEDOT:PSS, polyacrylic acid (PAA), and MXene. In this system, the hydrophobic aggregation microregions within the PAA crosslinked PEDOT:PSS dissipated energy in response to the external stress, while the 2D MXene introduced abundant intermolecular interactions and formed a conductive network within the hydrogel. As a result, the resulting composite hydrogel exhibited enhanced mechanical properties and conductive performance[110]. In another study, an elastic, conductive ($\sigma > 140 S/cm$) and highly stretchable ($\varepsilon > 600\%$) composite material with a low Young's modulus ($E < 7 MPa$) was developed. In this composite, PEDOT:PSS served as the conductive component, while PU functioned as an elastomer. Additionally, the ionic liquid EMIM:tricyanomethanide (TCM) not only enhanced the mechanical and conductive properties of the composite but also facilitated the aqueous dispersion of PU through its ionic groups[111]. A recent study demonstrated that the multicomponent interaction within a PEDOT:PSS composite— comprising graphene, sodium dodecyl sulfate (SDS), and bis(trifluoromethane)sulfonimide lithium salt (BSL)—enables exceptional electrical conductivity exceeding 4000 S/cm. This performance approaches the conductivity range of metallic materials through a combination of complementary mechanisms: graphene establishes conductive pathways, SDS optimizes component dispersion and interfacial contact, while BSL enhances charge carrier mobility through ionic coordination effects[112]. Future work should explore synergistic interactions among additives, considering physicochemical properties, ratios, and printing methods for specific applications.

Advanced fabrication techniques for PEDOT:PSS-based bioelectronics

The widely investigated PEDOT:PSS-based bioelectronics for brain monitoring and modulation are mainly in the formats of hydrogels (Fig. 3a–c) or thin films. Hydrogels provide excellent mechanical softness, which is critical for interfacing with delicate neural tissues. They also have high water content, which helps mimic the natural environment of the brain and improves tissue integration, reducing the risk of inflammation or scarring[113]. Thin-film bioelectronics are fabricated onto rigid conductive (Fig. 3d–f) or flexible substrates (Fig. 3g–i). The conductive PEDOT:PSS deposited on flexible substrates, such as PDMS[114], can reduce the stiffness and thus decrease the mechanical mismatch with brain tissue. Meanwhile, the conductive PEDOT:PSS can be deposited on traditional rigid conductive substrates (e.g., metal-based substrates[115]) when the conductive PEDOT:PSS film can serve as a buffer layer that enhances the charge transfer efficiency and provides a relatively smoother, more biocompatible interface than rigid metal substrates for interaction with neural tissue. The next part in this section will discuss the well-investigated 3D and 2D technologies to construct PEDOT:PSS bioelectronics and what requirements these technologies impose on the properties of PEDOT:PSS materials.

3D printing technologies for bioelectronic fabrication

3D printing, also known as additive manufacturing, is a process that constructs a wide range of three-dimensional objects by layering materials based on a digital model. Unlike traditional manufacturing methods, which often involve material subtraction (e.g., cutting or drilling), 3D printing builds objects from the ground up, offering high versatility and material efficiency, especially for producing complex geometries[104]. 3D printing of PEDOT:PSS-based hydrogels enables the fabrication of intricate, flexible, and conductive structures suitable for various biomedical and electronic applications, including brain modulation. The ability to tailor the properties of PEDOT:PSS-based materials to align with printing requirements, and precise control over process parameters, makes 3D printing a highly promising approach for developing soft, conductive materials with intricate designs. Three prominent printing technologies—direct ink writing, inkjet printing (IJP), and vat polymerization (VP), demonstrate distinct capabilities and constraints in processing this water-soluble conductive polymer.

Direct ink writing (DIW) specializes in extruding soft, viscoelastic hydrogels with moderate resolution (50–400 μm)[116]. DIW requires the ink with shear-thinning behavior (viscosity: 1–1000 Pa·s at shear rates 1–100 s^{-1})[117]. For printing PEDOT:PSS-based bioelectronics, optimized ink formulations (5 wt% solid content) can balance extrudability and shape retention, minimizing lateral spreading while maintaining high conductivity and stretchability[118,119]. However, pure PEDOT:PSS has a solid content of less than 1.3%, so it cannot be directly used for DIW[30]. It requires several ink engineering, including solvent evaporation[120] and freeze-thawing[121], to increase the solid content. Meanwhile, viscoelastic polymers and conductive fillers can be added to the ink to tune its rheological properties[122]. DIW devices provide flexible process parameter control. Ian et al. investigated the effects of printing orientation, the temperature of the supporting platform, and nozzle diameter on the conductivity of printed PEDOT:PSS products. The results showed that the printing direction parallel with the direction of current flow could achieve a lower resistance than the perpendicular direction. Increasing the platform temperature can increase the PEDOT π–π stacking peak intensity and crystallite size, inducing higher conductivity

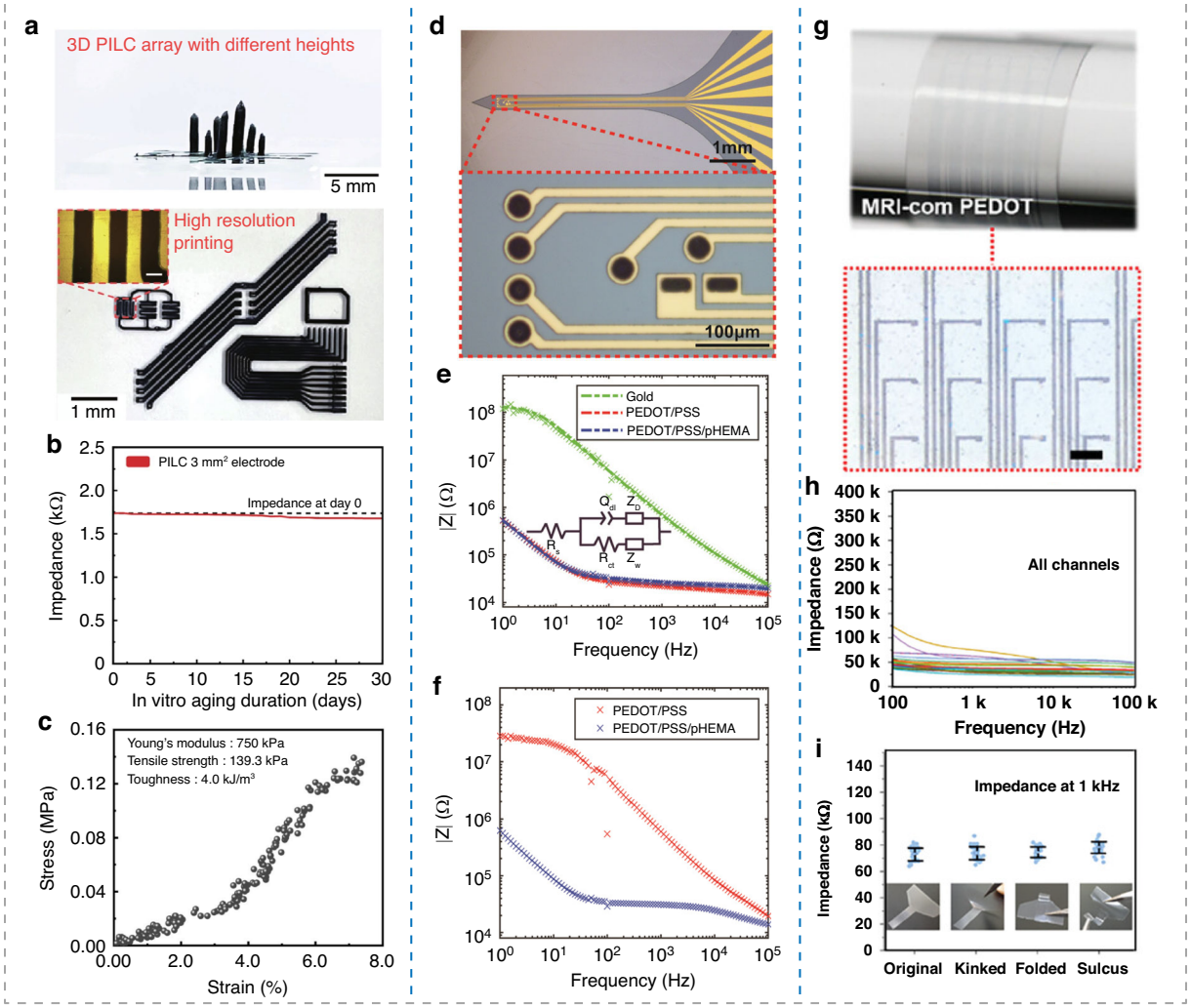

Fig. 3 Different formats of PEDOT: PSS-based electrodes. a–c PEDOT:PSS-ionic liquid colloidal (PILC) ink for 3D-printed hydrogel[45]. Copyright 2024, Springer Nature (Fig. S1). a: Images of a 3D array with a high aspect ratio (top) and high resolution (~50 μm) (bottom) fabricated via direct ink writing. **b** Impedance stability of PILC electronic devices incubated in PBS solution at 37 °C over 30 days. **c** Mechanical properties of printed PILC hydrogel, exhibiting a low Young's modulus (750 kPa), comparable to biological tissues. **d–f** PEDOT:PSS/pHEMA film deposited on a rigid metal substrate (Au electrode) via electrochemical deposition for microelectrode array (MEA) fabrication[165]. Copyright 2022, John Wiley and Sons (Fig. S2). **d** Images of the MEA shank (top) and a zoomed-in view of the pattern at the MEA tip (bottom). Gold: Au electrode; Black: PEDOT:PSS/pHEMA film. **e** Electrochemical impedance spectroscopy (EIS) measurement from 1 Hz to 100 kHz of bare gold MEAs (green), PEDOT/PSS (red), and PEDOT/PSS/pHEMA-coated (blue) MEAs. **f** EIS measurement of PEDOT/PSS (red) and PEDOT/PSS/pHEMA-coated (blue) during ageing test in PBS solution at 60 C for 7 days. **g–i**: PEDOT:PSS film deposited on a flexible substrate (PET) via spin coating[179]. Copyright 2023, John Wiley and Sons (Fig. S3). **g** Images of a transparent PEDOT:PSS-based ECoG grid wrapped around a cylindrical glass rod (5 mm diameter) (top) and a zoomed-in view of the electrode array (bottom). **h** EIS of the 30-channel ECoG grid. **i** Mechanical stability test of the ECoG grid, showing stable EIS values across 30 channels in four different states: original, kinked, folded, and sulcus

but the effects can be removed after DMSO treatment. Additionally, the nozzle size didn't significantly influence the conductivity of the printed PEDOT:PSS modules[123].

Inkjet printing (IJP) achieves high-resolution printing (feature sizes <50 μm) via precision droplet deposition (droplet volume <10 pL, spacing 1–7 μm), suitable for patterning microelectrode arrays[124]. Its non-contact approach minimizes ink waste and supports multi-material deposition on flexible/metallic substrates[125,126]. However, stringent viscosity limits (2–30 cP) necessitate PEDOT:PSS dilution, compromising conductivity[127,128]. Surfactants (e.g., SDS) stabilize jetting and improve substrate wettability but may introduce biocompatibility concerns[129].

Vat Polymerization (VP), particularly two-photon polymerization (2PP), enables fast fabrication of

photocurable hydrogels with submicron resolution (<1 μm)—unmatched by DIW or IJP[130]. This capability is critical for fabricating miniaturized neuromodulation devices (e.g., fractal electrodes) requiring microscale feature control. Photocurable resins, such as PEGDA, PEGDMA, and PVAMA are preferred in printing PEDOT:PSS-based bioelectronics via VP owing to their high hydrophilicity and biocompatibility[131]. To achieve relatively high conductivity, the weight ratio of PEDOT:PSS and photocurable resin is generally in the range of 2:3–1:1. A higher ratio of PEDOT:PSS may reduce the ink's printability, but a lower ratio may decrease the conductivity of bioelectronics due to the insulating property of photoresins[105,132]. Among the three methods, DIW is currently the most widely adopted 3D printing method for fabricating PEDOT:PSS-based bioelectronics in brain modulation. DIW dominates due to its unparalleled versatility in processing shear-thinning PEDOT:PSS hydrogels, enabling the fabrication of ultrasoft, mechanically compliant constructs that seamlessly interface with brain tissue. Unlike IJP—which suffers from conductivity compromises due to mandatory ink dilution and surfactant additives—DIW retains higher PEDOT:PSS loading for superior charge transfer while achieving moderate resolution (50–400 μm) sufficient for macroscale neural interfaces (e.g., cortical surface electrodes). While VP (notably 2PP) offers submicron precision for microscale features, its reliance on photocurable resins restricts PEDOT:PSS content, drastically reducing conductivity. DIW's compatibility with functional additives (e.g., carbon nanotubes, bioactive polymers) and scalable workflow further solidify its preference for creating implantable, tissue-integrated devices that balance conductivity, structural complexity, and chronic biocompatibility—critical requirements absent in IJP's or VP's material-process trade-offs.

2D printing technology for fabricating bioelectronics

2D fabrication methods focus on depositing uniform, conductive PEDOT:PSS layers onto flexible or rigid substrates. Among established techniques, spin coating and electrochemical deposition dominate due to their scalability, industrial compatibility, and ability to tailor material properties for neural interfaces.

Spin coating offers a cost-effective and scalable approach to deposit ultrathin (<100 nm), homogeneous PEDOT:PSS films on diverse substrates (flexible or conductive substrates)[133]. This method is particularly suited for planar bioelectronic devices, such as electrocorticography (ECoG) grids, where large-area, low-impedance coatings are essential for high spatial resolution and signal fidelity in cortical signal recording.

Electrochemical deposition (also called electropolymerization) enables site-specific, conformal growth of PEDOT:PSS on conductive substrates (e.g., Pt and Au)[134]. By directly integrating PEDOT:PSS with metallic microelectrodes, this technique reduces interfacial impedance by up to 90% and significantly improves signal-to-noise ratios[135]. These attributes make it indispensable for chronic neural implants, such as deep-brain stimulation electrodes, where stable, low-impedance interfaces are critical for long-term electrical recording and stimulation without performance degradation.

2D techniques (e.g., spin coating and ECD) excel in depositing uniform, thin conductive layers on planar or rigid substrates, offering high throughput, precise thickness control, and compatibility with industrial workflows, but lack structural complexity and tissue-like mechanical compliance. 3D printing (DIW, IJP, and VP) enables fabrication of customizable 3D architectures with soft, hydrogel-like mechanics that better mimic neural tissue, though at the cost of higher material complexity (e.g., ink engineering for rheology) and trade-offs between printability and conductivity. And its resolution limitations (generally >50 μm) restrict single-cell-level precision. Thus, method selection hinges on application priorities: 3D techniques are preferred for chronic, conformal interfaces (e.g., cortical surface conformers), whereas 2D methods remain indispensable for acute, high-fidelity devices (e.g., penetrating microelectrodes) demanding subcellular feature control.

Postprocessing

Postprocessing methods are crucial for enhancing the properties of PEDOT: PSS-based devices, such as conductivity and mechanical flexibility. Among these methods, thermal annealing is the most commonly used. It can increase the PEDOT:PSS matrices' crystallinity and enhance mechanical strength by increasing interlayer adhesion[136]. This process also removes excess and bound water, shrinking the insulating PSS regions and inducing structural rearrangements that boost conductivity. However, controlling the annealing temperature is critical. It should generally exceed 100 °C, with higher temperatures requiring shorter annealing times. But excessively high temperatures can degrade polymers, and different PEDOT:PSS formulations with various additives have different thermal stabilities[137]. Therefore, annealing conditions must be optimized for each specific PEDOT:PSS formulation. Solvent treatment, such as acid or DMSO treatment, can also enhance conductivity through a doping effect illustrated in section 1.1. Additionally, photocuring promotes the crosslinking of photosensitive polymers, increasing molecular interactions and forming a network that improves mechanical properties.

Applications of PEDOT: PSS-based conductive biomaterials for brain monitoring and regulation

PEDOT:PSS-based devices have emerged as versatile tools in neuroscience and clinical applications, spanning invasive, semi-invasive, and non-invasive paradigms. The PEDOT:PSS-based materials are particularly valuable in neural electrode design, where they enhance signal detection and modulation capabilities—critical for elucidating neural network dynamics, advancing cognitive research, treating neurological disorders, and enabling brain–computer interfaces (BCIs). By integrating PEDOT:PSS as a coating layer, electrodes achieve reduced electrical impedance, improved biocompatibility (mitigating immune responses), and enhanced mechanical flexibility, ensuring better conformability to neural tissues. Additionally, PEDOT:PSS serves as a standalone conductive interface in substrate-free electrodes, further simplifying device architecture. These innovations have been validated across diverse modalities: invasive implants for high-resolution neural recording, semi-invasive grids for cortical surface mapping, and non-invasive wearables for electrophysiological monitoring. Such applications highlight their dual utility in both fundamental research—such as probing neural circuit functions—and clinical translation, including diagnostics, neuromodulation therapies, and BCI development. As a result, PEDOT:PSS-based electrodes represent a transformative advancement in bridging technological performance with biological compatibility, offering scalable solutions for understanding and interfacing with the nervous system[138].

Invasive recording and stimulation

Invasive neural interfaces are indispensable tools for high-resolution brain activity mapping and targeted neuromodulation. Invasive recording captures neural signals across spatial scales—from single neuron action potentials to synchronized assemblies[139,140]—enabling precise functional analysis for neurological disorder diagnosis and therapeutic planning[140]. Similarly, invasive stimulation techniques like deep brain stimulation (DBS) modulate dysfunctional circuits through continuous/episodic electrical impulses, offering clinical solutions for conditions such as Parkinson's disease[141]. For invasive neural recording and stimulation, an electrode with a moderate modulus possesses sufficient stiffness for precise insertion into targeted brain regions while maintaining flexibility to minimize tissue damage caused by mechanical mismatch with the surrounding soft neural tissue. This mechanical balance is critical for preserving structural integrity during implantation and reducing chronic inflammatory responses. Simultaneously, low electrical impedance (<10 kΩ at 1 kHz) is essential to enhance signal fidelity during neural recording. However, conventional metal electrodes face critical limitations: (1) Mechanical mismatch (Young's modulus ~10–100 GPa vs. brain tissue ~1–4 kPa[10]) induces chronic inflammation and glial scarring, increasing interfacial impedance and signal attenuation[142]; (2) High impedance (>1000 kΩ at 1 kHz) (3) Electrochemical corrosion and inflammatory cytokine release cause neuronal loss near implants, degrading recording fidelity over time[143]. PEDOT: PSS-based electrodes address these challenges through three synergistic advantages: (1) Mechanical compatibility: a moderate rigidity (modulus ~100-1000 kPa) ensuring accurate penetration when minimizing insertion trauma and chronic foreign body response. (2) Electrochemical superiority: high conductivity (>100 S/cm) and low interfacial impedance (generally <20 kΩ at 1 kHz) enhance SNR and CIC for stable recording/stimulation. (3) Biostability: robust resistance to physiological degradation maintains performance over months, unlike corroding metal interfaces[25,144].

Single-unit recording

Single-unit recording, the most precise recording method in neuroscience, can catch the intracellular firing patterns of neurons and the extracellular spiking activity of neurons in the vicinity of the deep electrodes[145,146]. Single-unit recording utilizes a micromanipulator to finely control the electrode position to target the specific neurons. For intracellular unit recording, the electrode penetrates the neuron and measures the difference in electrical potential between the inside of the neuron and the extracellular fluid, where an external reference electrode is placed. For extracellular unit recording, the electrode detects voltage changes in the extracellular space caused by the target neuron's activity[147,148]. The typical device for single-unit recording is microelectrodes (MEAs). The ideal MEAs should have minimal size and interface impedance to record the maximally localized and high-quality signal. However, reducing electrode size inherently elevates interfacial impedance due to reduced effective surface area, thereby amplifying thermal noise and degrading SNR[149]. The application of PEDOT:PSS coatings to MEAs improves electrode performance through two synergistic mechanisms: surface roughening that expands the effective contact area, and a dual electrical-ionic conduction pathway that optimizes charge transfer kinetics at the electrode-tissue interface, collectively resulting in significant impedance reduction [150]. Du et al. compared the neural recording performance of bare gold electrode and PEDOT:PSS-coated gold electrode. The mean impedance values of gold MEA and PEDOT:PSS-gold MEA at 1 kHz were 1449 and 52 kΩ, respectively. Despite the PEDOT:PSS-coated MEA's impedance remaining suboptimal, the decreased impedance made the PEDOT:PSS-coated MEA showing relatively distinct extracellular active potentials with

distinguished waveforms and sortable units on each channel when the signal recorded by gold MEA had negligible active potentials with very low amplitude and high noise[151]. Although the thin and conductive PEDOT:PSS coating can lower the impedance, the rigid and stiff metal core may still cause mechanical mismatch with soft brain tissue, potentially leading to tissue damage or glial scarring over time. To resolve the problem, Yuk et al. developed a soft neural probe based on 3D-printed PEDOT:PSS hydrogel for in vivo single-unit recording. The dry-annealed PEDOT:PSS microstructures can be readily converted into a soft (Young's modulus <1.1 MPa) and conductive (electrical conductivity up to 28 S/cm) PEDOT:PSS hydrogel via subsequent swelling in a wet environment. After being implanted into the mouse dorsal hippocampus, the soft electrode could record distinctive action potentials in a freely moving mouse over 2 weeks[14]. Similarly, Zeng et al. designed an integrated all-hydrogel electrode for single neuron recording, but the conductivity increased by nearly 150 times. The design took advantage of the interaction between the positively charged primary amine group on dopamine and the negatively charged sulfate group on PSS to break the Coulombic interaction between conductive PEDOT and insulating PSS to promote the formation of ordered PEDOT chains. Next, the laser was applied to induce further phase separation to increase the PEDOT crystallinity. The two strategies significantly enhance the conductivity of the hydrogel up to 4176 S/cm. Meanwhile, the dynamic bonds provided by dopamine, combined with the hydrogel's porous structure, bolstered its flexibility and promoted effective stress dissipation. The conductive hydrogel was then incorporated into a 16-channel MEAs, recording signals from individual or multiple neurons. Unlike the rigid Ag electrode, the all-hydrogel neural electrode didn't cause any observable tissue damage and inflammation response after 14-day implantation, making it a promising tool for neural research[152]. In addition to electrical signals, the electrochemical detection of neurotransmitters, particularly dopamine, plays a crucial role in understanding neural system functions, with electrochemical methods serving as the primary approach for dopamine measurement and analysis. Wang et al. developed a multifunctional MEAs with PEDOT:PSS-based conductive materials and calcium alginate and chitosan crosslinked network coated with a Nafion cation-exchange membrane for synchronized measurement of neural activity signal and dopamine level. And the composite hydrogel was loaded with the anti-inflammatory drug dexamethasone sodium phosphate to decrease the post-implantation inflammatory reaction. The MEAs was implanted into the ventral and dorsal hippocampal areas of mice and could stably record the single neuron discharges in 17 days and monitor the dopamine level in 7 days. The dual-mode neural activity detection provided new insights for detecting single neuron activity[138].

Intracortical recording

Intracortical recording technology allows for direct measurement of neural activity from populations of neurons, including both action potentials (spikes) of individual neurons and local field potential (LFP), which reflect the slower, synchronized activity of many neurons working together[153]. The process involves that the electrodes are inserted into the target brain tissue under control and record summed electrical activity. Intracortical recording primarily relies on extracellular electrodes, including metal probes and microelectrode arrays (MEAs). However, as discussed previously, conventional metal electrodes face several limitations: elevated impedance in physiological environments, inadequate biocompatibility, and mechanical mismatch with neural tissue. To address these challenges, researchers have developed advanced PEDOT:PSS-coated electrodes with enhanced performance. For example, Li et al. utilized PEDOT:PSS-coated Pt nanoparticle composites to fabricate MEAs for investigating the role of the hippocampus and the Barrel Cortex in spatial navigation. The PEDOT:PSS coating significantly reduced the impedance of Pt MEAs, demonstrating a substantial decrease from 21 kΩ to about 3 kΩ at 1 kHz[154]. To improve the biocompatibility and softness further, the MEA fabricated from a 3D interpenetrating conductive polymer network was developed. The hydrogel network composed of crosslinked PEDOT/PSS/PVA exhibited a porous structure, empowering the MEA with good flexibility (Young's modulus about 191 kPa) and stretchability (72% strain). Then the MEAs were implanted into the dorsal hippocampus of rats, and the spontaneous action potentials were recorded before and during the light stimulation. The MEAs displayed good biocompatibility in vitro and in vivo and kept the neural recording capacity for up to 12 weeks[155]. Intracortical recording is an effective tool not only for investigating neural network dynamics and connectivity, but also for studying abnormal electrical activity in neurological disorders. Owing to the good conductivity and biocompatibility, PEDOT:PSS-based MEAs have been applied in monitoring the change of striatal electrophysiological activities during epileptic seizure[156,157], and abnormal neuroactivity of the delta band and beta band in Parkinson's disease model mice[158]. Multimodal detection of neural electrophysiological signals and neurotransmitters is meaningful to study the neurodynamic process in detail. Lu et al. prepared MEAs based on the composite of PEDOT:PSS, Pt NPs, and MWNCT for electrical signal detection and modified with Nafion film for dopamine detecting. The π–π conjugation between the conjugated PEDOT and MWNCT made the

PEDOT:PSS with good arrangement on the electrode, which increased the electrodes' conductivity and charge transfer ability. These properties enable the electrode to achieve a detection limit of 0.05 μM for DA detection, with a wide linear range of 0.05 to 70 μM. For in vivo validation, the optimized electrodes were surgically implanted in specific brain regions of sleep-deprived rat models targeting the right lateral cortex and caudate putamen (CPU) for simultaneous recording of dual-mode neural signals. The synchronous measurement of neurochemical and neurophysiological signals provided a good reference for multimodal neural activity detection for neurologic disease diagnosis and monitoring[159].

Intracortical stimulation and recording

Simultaneous intracortical stimulation and recording allow researchers to both stimulate and record neural activity within the same brain region or across multiple regions at high spatial and temporal resolution, providing a powerful technique to investigate the functional properties of neural circuits, brain plasticity, and the causal relationships between neural activity and behavior[160]. For intracortical electrical stimulation, small currents are applied through electrodes to make the neurons depolarized or hyperpolarized[161]. Simultaneously, neural activity (e.g., spikes and LFPs) is recorded from the same or nearby electrodes. MEAs serve as the standard tool for invasive brain stimulation and recording, leveraging their multi-site architecture to enable high-density electrophysiology and spatially targeted neuromodulation. For electrical stimulation, two parameters govern performance: charge storage capacity (CSC) and charge injection capacity (CIC). CSC has a minimum threshold of 0.5 mC/cm^2 for effective stimulation, quantifying the total charge stored at the electrode-electrolyte interface[162]. CIC demonstrates an electrode's capability to cause stimulation, where CICmax is the utmost charge quantity allowable for injection or transmission, beyond which irreversible electrochemical reactions, risking electrode or tissue damage, may occur[163,164]. Reportedly, applying a PEDOT:PSS coating enhances the CSC and CIC of silicon MEAs, thanks to its porous structure and large effective surface area. After depositing PEDOT:PSS, the CSC went up to 1.00 mC/cm^2 from 0.14 mC/cm^2. Additionally, PEDOT:PSS modification raised the MEAs' CICmax, as seen in the electrode potential increasing from −1.54 to −0.20 V, ensuring safe stimulation (>−0.6 V). The MEAs can deliver electrical stimulation to effectively control mice's movements. Plus, the implanted MEAs can accurately record spike potentials and LFP with high efficiency due to decreased impedance[164]. Although the PEDOT:PSS deposition can enhance MEAs' ability to perform stimulation and recording, the MEAs are still rigid and have a high Young's modulus (up to 1 GPa), causing a mechanical mismatch with brain tissue and brain damage. To solve the problem, Gary et al. coated a layer of poly(2-hydroxyethyl methacrylate) (pHEMA) hydrogel on top of the PEDOT:PSS, which was deposited on gold substrates. The resulting MEAs increased CSC (~12 mC/cm^2) and CICmax (3.3 mC/cm^2) compared with a bare gold electrode. The MEAs had a suitable Young's modulus (322 kPa) to conform to the soft brain tissue, achieving electrical stimulation and spontaneous recording on the dentate gyrus region of the hippocampus in free-moving rats for 21 days[165]. Another strategy to reduce brain damage is to perform the intracortical stimulation and recording via less invasive way. Ilke et al. developed high-density (40 μm pitch) high-capacitance (>1 nF) electrocorticography (ECoG) MEAs based on PEDOT:PSS, which could induce deep brain stimulation and related signal recording by being placed on the cortical surface. The high-volume-capacitance coating allows the electrodes to deliver larger amounts of charge within safe limits, generating strong electric fields in deep tissue, with current amplitudes between 45 and 60 μA targeting depths from 220 to 280 μm. The bipolar stimulation configuration confines the electric field between the electrodes, reducing current spread and enabling precise spatial tuning of neuronal responses (Fig. 4a–c)[166]. Although simultaneous intracortical stimulation and recording is a powerful technique in neuroscience and neuroengineering, enabling closed-loop systems for neural circuit studies, one severe challenge arises due to the interplay between stimulation and recording processes. The stimulation pulse creates a high-amplitude electric field, inducing currents in nearby recording electrodes, causing electrical artifacts. Liu et al. developed a new paradigm for neuron stimulation and neuron activity recording to avoid the stimulation artifacts. The intricate implantable microbe system was composed of microscale light-emitting diode (micro-LED) and PEDOT:PSS-coated diamond film to achieve optogenetic stimulation and electrical activity monitoring in the deep brain of mice (Fig. 5a–c)[167].

Semi-invasive mapping and stimulation

Semi-invasive brain mapping and stimulation methods enable neuromodulation with minimal disruption to brain tissue, which bridges the gap between fully invasive techniques and non-invasive techniques. The methods are widely used in clinical and research settings for diagnosing neurological disorders, mapping brain functions, and developing brain–computer interfaces (BCIs). Compared to fully invasive brain modulation, semi-invasive methods realize large-scale modulation with less invasiveness. Meanwhile, semi-invasive methods achieve relatively higher spatial resolution and sensitivity than non-invasive ways in which signals pass

through the skull and scalp, causing attenuation, and slurring[168,169].

Cortical mapping

Electrocorticography (ECoG) serves as a principal technique for semi-invasive brain mapping, utilizing electrode arrays positioned either directly on the cortical surface (subdural) or above the dura mater (epidural) to capture electrophysiological activity with high spatial and temporal resolution[168]. Modern ECoG systems employ high-density electrode grids or MEAs engineered to meet two critical requirements: (1) micron-scale spatial resolution for precise mapping of localized cortical activity, and (2) low interfacial impedance (ideally <10 kΩ at 1 kHz)[170] to ensure optimal SNR for reliable neural signal acquisition. These electrode arrays must additionally maintain conformal contact (modulus: ~10–100 kPa) with the brain's complex surface topography. Recent advances in material science have demonstrated the efficacy of PEDOT:PSS-based ECoG electrodes, which offer superior performance characteristics including significantly reduced impedance, good conformity, enhanced biocompatibility, and scalable fabrication through solution-processable manufacturing. Mehran et al. developed PEDOT:PSS-based electrode arrays that exhibited more than tenfold lower impedance and a narrower impedance distribution compared to Pt electrodes. These arrays demonstrated enhanced differential power detection and achieved precise spatial resolution, mapping cortical activity at distances as small as 400 µm, outperforming clinical Pt electrodes in patient studies[171]. Oh et al. advanced DIW-based bio-fabrication by developing 3D PEDOT:PSS-ionic liquid colloidal (PILC) electrodes, where ion-exchange-induced hydrogen bonding network formation between ionic liquids and PEDOT chains yielded tunable rheology for precise printing while enhancing electrical conductivity (286 S/cm) and flexibility (105 kPa storage modulus). A post-fabrication purification process via centrifugation eliminated residual ionic components, achieving <5% cytotoxicity, while the optimized architecture enabled dose-dependent neural response amplitudes to varying stimulation intensities[45]. To achieve recording with high spatial resolution, high electrode density, and small electrode size is necessary. Li et al. engineered a flexible 14-channel MEA array on a 60-µm-diameter substrate based on PEDOT:PSS and MWCNT, achieving high-density cortical mapping through micron-scale spatial resolution and low interfacial impedance (<20 kΩ at 1 kHz). Implanted across rat cortical networks spanning somatosensory, parietal association, and visual cortices, the array demonstrated differential electrocorticography (ECoG) signatures between baseline and epileptiform states, revealing state-specific alterations in theta-band power (about tenfold increase during seizures). This minimally invasive platform enables precision neuro-diagnostics, showing translational potential for both epilepsy focus identification (validated against histopathology) and functional network mapping in neurodegenerative disorders[172]. Recent advances in multimodal neurotechnology integrate transparent microelectrodes with optical imaging modalities, enabling simultaneous electrical recording and cellular-resolution visualization of neural circuits[7]. Mary et al. engineered a cortical interface using PEDOT:PSS on parylene-C substrates, achieving dual functionality through unencumbered optical access (920 nm) for two-photon imaging and low interfacial impedance (25 kΩ at 1 kHz) for stable electrophysiological monitoring[173]. In a similar development, Gerwin et al. implemented a novel photolithographic patterning strategy utilizing fluorinated photoresist with optimized gap exposure protocols, which preserved PEDOT:PSS conductivity (3.5 kΩ at 1 kHz) while maintaining 75% optical transparency across visible wavelengths[7]. Building upon the proven efficacy of PEDOT:PSS-based cortical interfaces, recent structural engineering efforts focus on optimizing electrode microarchitecture. Ji et al. compared the performance of PEDOT:PSS modified flat electrodes and wrinkled electrodes. There was little difference in impedance between the wrinkled electrode and the flat one, while the wrinkled electrode exhibited higher electrochemical stability than the flat electrode. In vivo experiment, both MEAs achieved similar ECoG recording ability. The authors attribute the constrained performance enhancement to suboptimal surface area amplification (33–42%) achieved through current wrinkle geometries, proposing a multiparameter optimization framework combining liquid elastomer composition tuning, rigid overlayer thickness control, and surface functionalization to achieve interfacial area expansion in their future work[135]. Rachel et al. engineered a highly ordered PEDOT-based block copolymer brush architecture (PSS-b-PPEGMEMA) via surface-initiated atom-transfer radical polymerization (SI-ATRP) strategy, achieving a unique combination of mechanical compliance (Young's modulus: 1.7 ± 0.6 MPa in aqueous conditions) and electrochemical performance (impedance: ~100 kΩ at 1 kHz). The molecular-scale alignment of polymer brushes created open ion/electron transport pathways, coupled with enhanced interfacial ordering, which synergistically improved charge transfer kinetics and stability—retaining 95% capacitance over 3500 electrochemical cycles, outperforming conventional crosslinked films that degraded after 2500 cycles. Crucially, the dense brush morphology exhibited superior conformal adhesion to biological surfaces (0 air gap formation) compared to spin-coated analogs, which suffered from delamination on soft substrates. This structural precision, validated by nanoscale imaging and

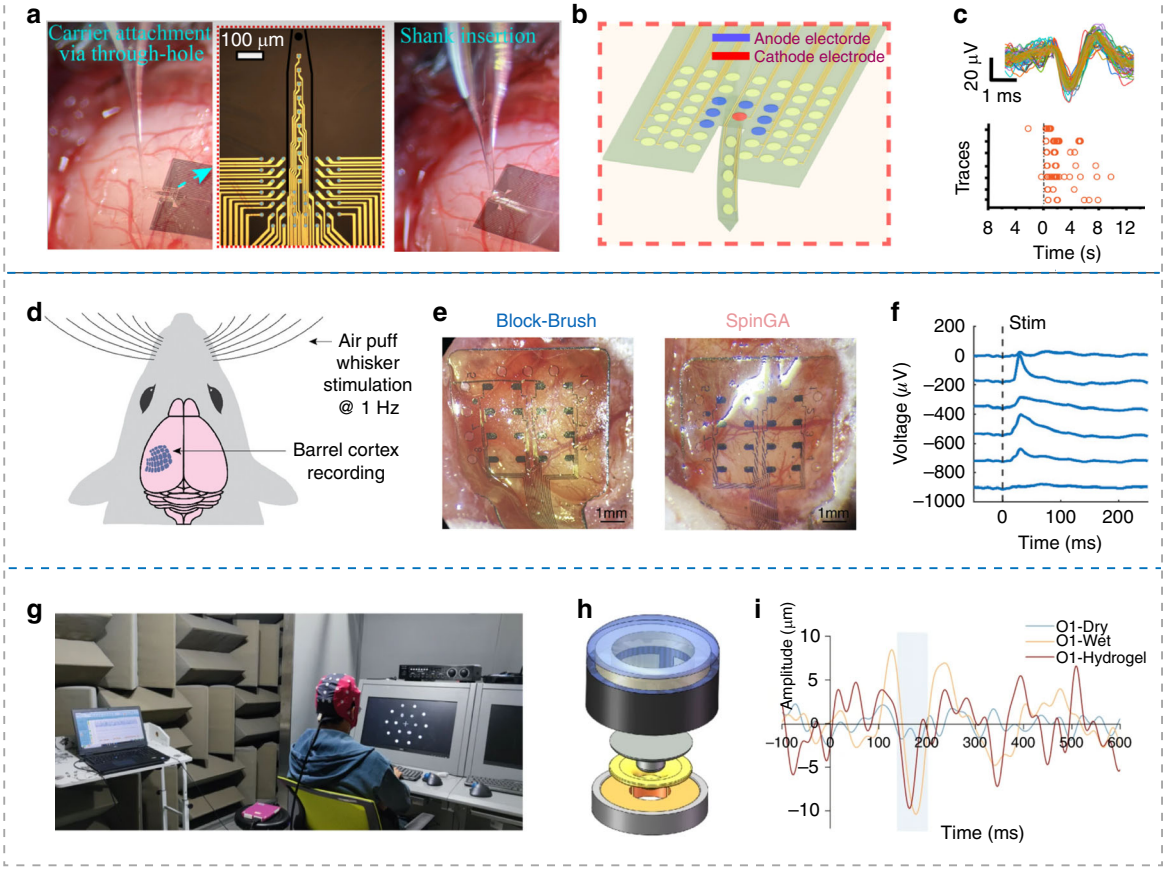

Fig. 4 PEDOT:PSS-based bioelectronics for invasive, semi-invasive, and non-invasive brain modulation approaches. PEDOT:PSS-based bioelectronics for invasive (**a**–**c**), semi-invasive (**d**–**f**), and non-invasive (**g**–**i**) brain modulation. **a**–**c** PEDOT:PSS thin-film microelectrode arrays (MEAs) for brain stimulation and single-unit recording[166]. Copyright 2022, The American Association for the Advancement of Science (Fig. S4). **a** The implantation process of a surface MEA (for surface stimulation) and a depth neuro-probe (for single-unit recording). Using a carrier glass pipette, the shank extension of the MEA was partially inserted into the brain, with ten electrodes reaching up to 500 μm below the pial surface. A micrograph of the MEA is shown (middle). **b** Illustration of the implanted MEA positioned both inside and on the brain surface, with PEDOT:PSS electrodes highlighted in blue. **c** Spike waveforms computed by averaging 50 traces recorded with the depth probe at 160 μm below the pial surface from a single neuron. **d**–**f** Block-Brush PEDOT:PSS film for ECoG recording[174]. Copyright 2024, John Wiley and Sons (Fig. S5). **d** Schematic illustration of a 16-channel array implanted on the surface of the rat brain for barrel cortex recording under air-puff whisker stimulation. **e** Microscope image of the electrode array on the surface of the brain. The Block-Brush structure produced by SI-ATRP exhibited excellent conformity with the brain surface, whereas the electrode film fabricated by spin coating (SpinGA) presented an air gap. **f** Stimulation responses recorded from six individual low-impedance channels in the Block-Brush array. The dashed line indicates the timing of air-puff stimulation. **g**–**i** PEDOT:PSS hydrogel-based electrode for EEG[189]. Copyright 2023, Springer Nature (Fig. S6). **g** A photograph of a subject undergoing EEG monitoring. **h** Illustration of the EEG electrode. **i** EEG waveforms recorded using hydrogel, wet, and dry electrodes. The signals from the hydrogel electrode closely resembled those from the wet electrode but differed from those recorded with the dry electrode

electrochemical impedance spectroscopy, establishes a new paradigm for durable bioelectronic interfaces where molecular-level control directly translates to stable device-tissue integration and long-term functional reliability (Fig. 4d–f)[174].

Cortical stimulation and mapping

Cortical stimulation and recording technologies deliver electrical stimuli to specific cortical regions while capturing the resulting neural activity. For safe, effective, and reliable operation, electrode arrays should exhibit excellent biocompatibility, mechanical flexibility, high CIC and volumetric capacitance, and low impedance. George et al. developed a biohybrid electrode by combining Aloe vera (AV) gel with PEDOT:PSS, creating free-standing, conformable films with hydration-tunable mechanical properties. These electrodes exhibited dynamic softening upon water absorption, enabling them to adapt to the rough, porous skull surface, while maintaining structural integrity after dehydration. The resulting conductive films demonstrated exceptional electrochemical performance, including a volumetric capacitance of 1.3 mF—over 200-fold higher than gold electrodes (5.5 μF)—supporting the hypothesis that the AV-PEDOT:PSS (AVCP) films achieve

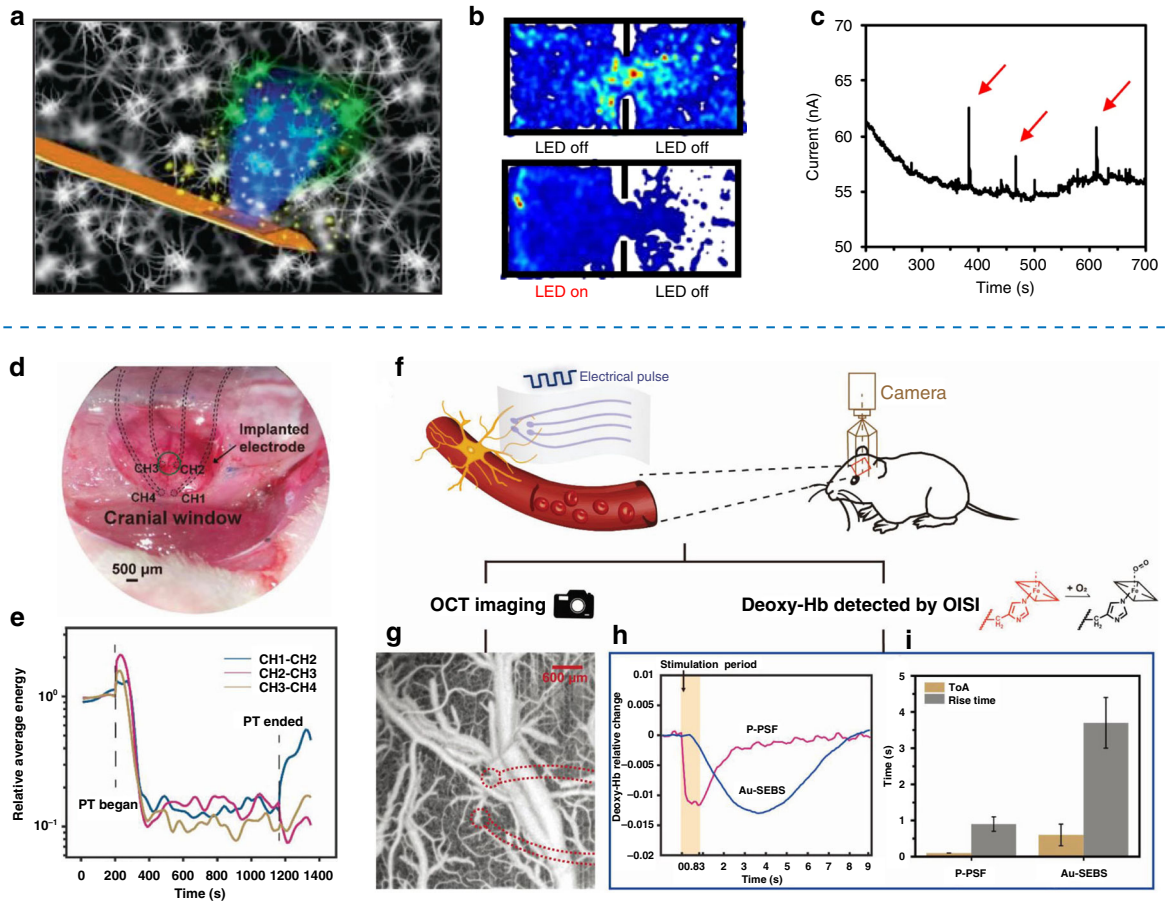

Fig. 5 PEDOT:PSS-based bioelectronics for multimodal brain modulation. a–c PEDOT:PSS-based microprobe system for optical stimulation and neurological activity sensing[167]. Copyright 2020, Springer Nature (Fig. S7). **a** Schematic illustration of the microprobe system for optical stimulation and electrochemical sensing in deep brain tissue. **b** Position heat maps of animal activity, where hotter colors indicate longer duration at a given site. The map reveals that mice exhibit clear place preferences during the optogenetic stimulation period. **c** Spontaneous current spikes recorded during optogenetic stimulation. **d–i** A transparent electrode array based on PEDOT:PSS crosslinked with PEGDE and silk fibroin (P-PSF) for dual-modal neural-vascular activity probing[178]. Copyright 2021, John Wiley and Sons (Fig. S8). **d** The transparent and conformable electrode was placed on the rat brain. **e** Time domain of neural electrical signals recorded from CH1-CH2, CH2-CH3, and CH3-CH4 showing changes during and shortly after photothrombosis (PT) stroke. **f** Schematic illustration of the transparent P-PSF electrodes for integrated vessel imaging and blood oxygen measurement under electrical stimulation. **g** Optical coherence tomography image of P-PSF electrodes (red dotted lines) positioned on the neurovascular system in the rat brain. **h** Relative changes in deoxy-Hb level in response to electrical stimulation induced by the P-PSF electrode compared to the referenced Au-SEBS electrode. **i** Statistical analysis of the time of arrival (ToA) and rise time upon stimulation

high capacitance through bulk charge storage mechanisms, in contrast to the surface-limited electrical double-layer capacitance of Au interfaces. In vivo testing showcased the electrodes' bidirectional functionality: they successfully induced focal seizures in mice by delivering high currents (~90 mA) and simultaneously recorded evoked neural activity, highlighting their potential for integrated neural stimulation and recording applications[175]. The multimodal integration of high-density electrocorticography (ECoG) arrays with advanced neuroimaging modalities such as, two-photon calcium imaging or functional magnetic resonance imaging (fMRI) enables correlative analysis of electrophysiological dynamics and mesoscale neural circuit mechanisms, bridging the critical gap between cellular-level activity and whole-brain network interactions to advance mechanistic understanding of cognitive processes[176]. Zheng et al. advanced neural interface fabrication through a coagulation bath-optimized DIW process, producing DBSA-doped PEDOT:PSS hydrogels with dual-phase molecular engineering: DBSA-mediated selective leaching of insulating PSS chains and solvent-assisted reconfiguration of PEDOT into π-conjugated crystalline domains. This yielded hydrogels with enhanced electrical conductivity (600 S/cm) and mechanical flexibility (Young's modulus: 1.5 MPa), enabling the creation of a four-channel micro

ECoG (μECoG) array featuring 200-μm-resolution electrodes that achieved high-performance stimulation metrics—CIC of 6.4 mC/cm^2 and low interfacial impedance (2.0 kΩ at 1 kHz). A thermal dry annealing protocol further enhanced substrate adhesion strength, facilitating the integration of calcium indicators (GCaMP6s) for multimodal cortex-wide interfacing[177]. Cui et al. engineered a multifunctional neural interface by integrating PEGylated silk fibroin (PSF) with PEDOT:PSS (P-PSF) through molecular interactions between the ethylene glycol/epoxy moieties of PSF and sulfonate groups of PSS, forming an interpenetrating polymer network. The P-PSF electrodes exhibited exceptional electromechanical performance, combining high stretchability (≈260% strain), transparency (>85% transparency across 400–1500 nm), low sheet impedance (160 ± 56 Ω/sq), and long-term stability (1.4-fold change of sheet impedance over 4 months in PBS solution). Their superior CIC (3.2 mC/cm^2) surpassed Au electrodes by three orders of magnitude, enabling precise neuromodulation. Being placed in the cortical region of the rat's brain, the P-PSF electrode could efficiently deliver electrical stimulation. During stimulation, P-PSF elicited immediate hemodynamic responses—time of arrival (ToA) <0.1 s and rise time (0.8 s) fully synchronized with the 0.83 s stimulation period, as evidenced by deoxygenated hemoglobin (deoxy-Hb) dynamics. In stark contrast, Au electrodes showed delayed activation (ToA: 0.6 s; rise time: 3.7 s), highlighting P-PSF's enhanced electrode-tissue coupling for real-time, artifact-free neurovascular interrogation (Fig. 5d–i)[178]. In a recent study, Young et al. developed a flexible, transparent PEDOT:PSS neural implant with MRI compatibility due to its lower conductivity compared to metal electrodes, minimizing RF-induced heating and image artifacts. Despite PEDOT:PSS-EG's reduced conductivity, its high surface area enhanced interfacial double-layer capacitance (0.7 mC/cm^2) and lowered impedance (25 kΩ at 1 kHz), enabling reliable electrophysiological recording. This system supported 30-channel recording under stimulation and artifact-free MRI, allowing simultaneous neural interfacing and imaging[179]. The integration of simultaneous cortical stimulation and imaging offers a powerful approach to precisely visualize and investigate how stimulation influences neural activity, underlying brain networks, and behavioral outcomes.

Non-invasive mapping and stimulation

Non-invasive paradigms are the main tools to monitor and modulate cortical plasticity in healthy awake human cortex[180]. Electroencephalography (EEG) is a widely applied non-invasive mapping method to record and amplify the electrogram of the spontaneous bioelectrical signals from the brain neural activity[181]. In EEG, electrodes placed on the scalp measure the absolute postsynaptic potentials produced by neurons, as well as the currents flowing in and around them[182]. Compared with invasive and semi-invasive signal recording technologies, EEG provides a safe and feasible approach to acquire the inherent rhythmic electrical activity of brain cluster cells, making it valuable in understanding brain's cognition mechanism, diagnosing neurological disorders, and developing brain–computer interfaces[181]. However, EEG signals are generally weak and susceptible to interference from other electrophysiological sources. To ensure signal quality, EEG electrodes must combine high conductivity, stability, and low contact impedance (ideally <10 kΩ within the 0.5–70 Hz frequency range). To be noted, impedances below 100 Ω are unacceptable, as they often indicate a shunt or short circuit caused by conductive gel bridging (salt bridges) on the scalp[183]. Zhao et al. developed an ultrathin (100 nm), highly conductive, and conformable skin electrode using a PEDOT:PSS-transferred CVD graphene film (PTG) for electrophysiological applications. To enhance conductivity and mechanical stretchability, sodium dodecyl sulfate (SDS) and bis(trifluoromethane) sulfonimide lithium salt (BSL) were incorporated into the PEDOT:PSS solution. The optimized PTG film achieved a conductivity of ~4142 S/cm and a reduced impedance of 32 kΩ at 100 Hz (vs. 45 kΩ for Ag/AgCl). Under 40% strain, PTG exhibited fewer cracks and less distinct parallel wrinkles than pure PEDOT:PSS, attributed to enhanced PEDOT alignment via π–π interactions with graphene. AFM characterization revealed a Young's modulus of ~640 kPa, aligning with human stratum corneum compliance (~150 kPa), ensuring mechanical compatibility with skin. In a 12-h EEG monitoring test on a volunteer's scalp, PTG electrodes maintained stable recordings during sleep, exercise, and calm recovery. Alpha and delta wave intensities were strongest during exercise, consistent with physiological activity, validating PTG's reliability for long-term monitoring under dynamic conditions[112]. The research group later designed a sandwich-structured electrode, confining PEDOT:PSS between two graphene oxide (GO) layers. The design achieved high conductivity of 3727 S/cm, enabling overnight EEG recording as a volunteer went through light sleep to deep sleep and returned to light sleep. Meanwhile, the appropriate transparency (80% at 550 nm) of the electrodes can be applied in functional near-infrared spectroscopy (fNIRs) for recording the change of hemoglobin at the same position of EEG recording, which provided reference for multimodal brain activity monitoring[184].

Brain–computer interface (BCI), also called brain-machine interface (BMI), is a direct communication link between neural activity generated by the brain and an

external device, such as a computer[185]. According to the signal acquisition modal, the BCI can be divided into invasive BCI and non-invasive BCI[186]. Considering the feasibility and safety, EEG based non-invasive method is most commonly used for BCI tests. The conventional electrodes for BCI include wet electrodes, dry electrodes, and semi-dry electrodes. Wet electrodes require conductive gel to improve signal quality and are widely used in clinical settings due to their high SNR[187]. Conductive polymer gels are usually applied as the channels in wet electrodes to offer an intimate interface between solid electronics and soft biological tissues. Yang et al. developed an injectable EEG electrode using a shear-thinning, self-healing PEDOT:PSS/PVA/borax hydrogel formed via shaking-induced crosslinking. The hydrogel exhibited softness (Young's modulus ~2.5 MPa), high stretchability, low impedance (~10 kΩ at 0.1 Hz), and high SNR (~14 dB), making it suitable for BCI applications. In tests with ten volunteers exposed to 500 visual stimuli, the hydrogel achieved accuracy and information transmission rates comparable to commercial wet electrodes. It retained performance after ten uses or 4-month storage and was easier to clean than conventional conductive pastes, positioning it as a practical substitute for commercial gels in BCI systems[109]. Although a wet electrode can achieve high SNR, the gel has to be cleaned after testing, which is time-consuming. In contrast, dry electrodes do not require gel, making them more user-friendly for non-clinical or wearable BCI applications[188]. However, they often exhibit lower SNR due to increased skin-contact impedance. To address this issue, semi-dry electrodes have been developed that use a minimal amount of liquid or gel to enhance conductivity while remaining less messy than wet electrodes. Xue et al. designed a semi-dry, double-layer hydrogel electrode featuring a conductive layer for ion/electron transport—incorporating PEDOT:PSS and KCl electrolytes—and an adhesive layer that ensures secure skin attachment. The conductive layer is crosslinked with sodium alginate (SA) and polyacrylamide (PAM) to enhance roughness, with its modulus tunable to 20 kPa by adjusting the SA-to-AM ratio for long-term comfort, and includes glycerol to retain hydration (over 50% water retention after 3 days). EEG signals are transmitted via chloride ion migration from the skin to Ag/AgCl electrodes. This innovative formulation achieved low impedance (<5 kΩ at 0.5–50 Hz) and enabled stable, continuous EEG monitoring for 12 h (Fig. 4g–i)[189].

Despite significant progress, challenges remain in scaling PEDOT:PSS-based technologies for clinical applications. Ensuring long-term stability and addressing biocompatibility concerns are critical. Moreover, integrating multifunctionality—such as combining electrical and optical capabilities—offers a promising pathway for innovation. Emerging fabrication techniques, including 4D printing and hybrid nanocomposites, are expected to further enhance device performance. Overcoming these hurdles could enable PEDOT:PSS-based bioelectronics to revolutionize neural interfaces, providing unprecedented insights into brain function and paving the way for advanced therapies and diagnostics.

Conclusions

PEDOT:PSS, as an outstanding organic conductive material, has emerged as a transformative tool in bioelectronics. It enables the fabrication of customized structures for specific applications and facilitates the integration of PEDOT:PSS with other materials to enhance biocompatibility and functionality. PEDOT:PSS has been extensively studied and utilized in neural interfaces for recording and stimulating brain activity. Its widespread adoption is primarily due to its biocompatibility, flexibility, and softness, making it well-suited for interfacing with the soft and delicate brain tissue. Additionally, PEDOT:PSS exhibits relatively high conductivity and low impedance that can be further enhanced with additives, improving signal fidelity for neural recording, neurotransmitter detection, and targeted brain stimulation. Furthermore, PEDOT:PSS can be processed using solution-based techniques, including 3D printing and 2D deposition, enabling the fabrication of application-specific structures and seamless integration with other materials to improve functionality. Moreover, its optical transparency offers a unique advantage for integration with other stimulation and detecting technologies, such as optical stimulation and fNIRs, enabling multifunctional capabilities for stimulation, recording, and visualization of neural activity.

Although PEDOT:PSS exhibits great promise in developing bioelectronics for brain modulation, several challenges limit its stable and long-term application. (1) In vivo degradation: A major limitation of PEDOT:PSS is its degradation in biological environments. The high hydrophilicity of PSS chains can cause swelling or delamination of PEDOT:PSS films in the brain's aqueous environment, leading to device failure. Crosslinking strategies have been explored to improve stability by introducing chemical bonds that interact with PSS chains[190]. For example, 3-hydroxymethyl-3-methyl-oxetane has been reported to enhance the water-resistance of PEDOT:PSS films by crosslinking with PSS[191]. Additionally, encapsulating PEDOT:PSS with a thin layer of biocompatible, water-resistant polymer could enhance its long-term stability. For instance, a passivation layer composed of primer and epoxy-based negative photoresist has been applied on top of the PEDOT:PSS layer to prevent water penetration[192]. (2) Poor adhesion to substrates: PEDOT:PSS films often suffer from weak adhesion, leading to delamination,

particularly under mechanical stress, which poses challenges for chronic implants. Adhesion can be improved by adding surfactants to the PEDOT:PSS solution or by treating the substrate surface with methods such as plasma treatment[193] or polydopamine treatment[194], both of which enhance wettability and bonding strength. (3) Lack of standard processing protocols: To optimize the conductivity and mechanical properties of PEDOT:PSS, additives, such as acid, DMSO, or ionic liquids, are commonly used. However, these additives can introduce toxicity and variability in fabrication, making it difficult to develop biocompatible and reproducible bioelectronics. To address this issue, excessive additives can be removed through techniques such as centrifugation[45], and standardized fabrication protocols should be established to ensure consistency and safety. Considering the rapid progress in PEDOT: PSS-based conductive biomaterials for neural interface, future efforts are needed to address existing challenges and drive advancements in the field. (1) Enhancing fabrication techniques and optimizing the formulation design: While 3D printing technology has shown great potential in printing intricate structures with tailored properties, most studies still rely on traditional 2D printing methods. Techniques such as spin coating, commonly used for PEDOT:PSS processing, are limited in their ability to produce complex, high-resolution structures. In the future, more advanced technologies, including 3D, 4D even 5D printing, can be leveraged to create sophisticated and densely packed MEAs for precise neural recording and stimulation[45]. Additionally, following quality-by-design principles, the process parameters of advanced printing technologies should be optimized based on the specific properties of different PEDOT:PSS-based inks to maximize critical quality attributes. Moreover, standardized protocols for PEDOT:PSS processing should be established to ensure consistent device performance across and reproducibility. (2) Development of multifunctional electrical interface: Current PEDOT:PSS-based devices for neural modulation primarily focus on electrical interfacing. However, recent studies have begun exploring the integration of PEDOT:PSS-based electrical modulation with optical modulation as well as imaging techniques[112,177,184]. This multifunctional approach aims to improve our understanding of brain function, advance treatments for neurological disorders, and enhance brain-machine interfaces (BMIs) by leveraging the strengths of multiple modalities within a unified platform. In the future, PEDOT:PSS-based neural interfaces can incorporate microfluidic channels for localized stimulation-triggered drug delivery, enabling simultaneous electrical stimulation and pharmacological intervention for neurological disorders[195]. Moreover, adaptive closed-loop brain state–dependent stimulation offers a promising strategy by dynamically adjusting stimulation parameters in real time based on the brain's activity or state[196]. Future research should focus on integrating PEDOT:PSS neural interface with closed-loop systems with advanced data processing systems to achieve precise, personalized, and real-time brain modulation. Such advancements could lead to more effective treatments for neurological disorders, including Parkinson's disease and major depression disorder. (3) Considerations about clinical translation: For the successful clinical application of PEDOT:PSS-based neural interfaces, several critical considerations must be addressed to ensure their safety, efficacy, and long-term stability. Key considerations include biocompatibility and cytotoxicity, electrochemical stability and durability, electrical performance and signal fidelity, mechanical stability and durability, environmental and thermal stability, long-term in vivo testing, and regulatory compliance. One significant challenge is the sensitivity of PEDOT:PSS to environmental factors, particularly humidity, which can alter its morphology and performance. Optimizing the material composition can help enhance stability. For example, Seong et al. demonstrated that crosslinking PEDOT:PSS with 3-glycidyloxypropyltrimethoxysilane reduces the styrene sulfonate content and increases polymer crystallinity, improving stability in aqueous environments[115]. Additionally, selecting an appropriate sterilization method is also critical to maintain the functions. Ilke et al. reported that autoclaving is a viable sterilization method for PEDOT:PSS electrophysiology devices, preserving morphology and causing minimal impact on electrical properties[197]. Radiation sterilization is another commonly used method. But different PEDOT: PSS-based electrical composites exhibit varying sensitivities to heat, moisture, and radiation. Therefore, sterilization protocols should be carefully optimized based on the specific composition and application of the device.

Achieving these objectives requires continuous advances in PEDOT:PSS composition optimization, neural interface structural design, and integration with other cutting-edge technologies, such as 3D printing and data processing. Additionally, refining testing methodologies is essential to ensure reliability and performance. We believe that further progress in these fields will lead to the development of safer, more stable, and multifunctional neural interfaces, making them accessible not only for scientific research but also for practical clinical applications.

Acknowledgements

This work was supported by the Hospital-level scientific research fund of Yunfu People's Hospital(A20231006), the Start-Up Fund for Introduced Talents and Scientific Research at Beijing Normal University (28709-312200502501), Overseas Expert Project of Guangdong Province (30802-110690303), National major project of brain science and brain-like research (2021ZD0204300), National major scientific research instrument development project (61827811), National Natural Science Foundation of China (22407015), Natural Science

Foundation of Guangdong Province (2024A1515012271), Guangdong Provincial Pearl River Talents Program (2023QN10Y223), the start-up funding from Beijing Normal University (312200502504), Macao Science and Technology Development Fund (FDCT 0020/2019/AMJ and FDCT 0048/2021/AGJ), University of Macau (MYRGGRG2023-00038-FHS and MYRG2022-00054-FHS), and Higher Education Fund of Macao SAR Government Natural Science Foundation of Guangdong Province (EF017/FHS-YZ/2021/GDST).

Author details
[1]Faculty of Arts and Sciences, Beijing Normal University, Zhuhai 519087, China. [2]School of Systems Science, Beijing Normal University, Beijing 100875, China. [3]School of Applied Physics and Materials, Wuyi University, Jiangmen 529020, P. R. China. [4]Central Laboratory of YunFu People's Hospital, Yunfu, Guangdong, China. [5]Centre for Cognitive and Brain Sciences, Institute of Collaborative Innovation, University of Macau, Macau SAR 999078, China. [6]Department of Psychology, Faculty of Arts and Sciences, Center for Cognition and Neuroergonomics, State Key Laboratory of Cognitive Neuroscience and Learning, Beijing Normal University, Zhuhai, China. [7]Beijing Key Laboratory of Applied Experimental Psychology, National Demonstration Center for Experimental Psychology Education (Beijing Normal University), Faculty of Psychology, Beijing Normal University, Beijing, China

Author contributions
The concept and framework of this review was designed by M.X. The manuscript was equally prepared by M.X., J.L., D.M. and J.H. J.G., Y.H., S.W., Z.L. and Z.Y. provided help in revising this manuscript. All authors have given approval to the final version of the manuscript.

Conflict of interest
The authors declare no competing interests.

Supplementary information The online version contains supplementary material available at https://doi.org/10.1038/s41378-025-00948-w.

Received: 19 December 2024 Revised: 14 March 2025 Accepted: 31 March 2025
Published online: 13 May 2025

References

1. Kim, M., Lee, H., Nam, S., Kim, D.-H. & Cha, G. D. Soft bioelectronics using nanomaterials and nanostructures for neuroengineering. *Acc. Chem. Res.* **57**, 1633–1647 (2024).
2. Long, Y., Li, J., Yang, F., Wang, J. & Wang, X. Wearable and implantable electroceuticals for therapeutic electrostimulations. *Adv. Sci.* **8**, 2004023 (2021).
3. Koo, J. H., Song, J.-K., Kim, D.-H. & Son, D. Soft implantable bioelectronics. *ACS Mater. Lett.* **3**, 1528–1540 (2021).
4. Li, J., Cao, J., Lu, B. & Gu, G. 3D-printed PEDOT:PSS for soft robotics. *Nat. Rev. Mater.* **8**, 604–622 (2023).
5. Li, G. et al. Highly conducting and stretchable double-network hydrogel for soft bioelectronics. *Adv. Mater.* **34**, 2200261 (2022).
6. Lee, J. & So, H. 3D-printing-assisted flexible pressure sensor with a concentric circle pattern and high sensitivity for health monitoring. *Microsyst. Nanoeng.* **9**, 44 (2023).
7. Dijk, G., Kaszas, A., Pas, J. & O'Connor, R. P. Fabrication and in vivo 2-photon microscopy validation of transparent PEDOT:PSS microelectrode arrays. *Microsyst. Nanoeng.* **8**, 90 (2022).
8. Grygiel, M., Ratyński, M., Czerwiński, A. & Hamankiewicz, B. PEDOT:PSS as a conductive polymer binder for ecologically and economically sustainable, carbon-free NMC electrodes. *Appl. Phys. A* **130**, 889 (2024).
9. Wang, Y., Yang, X., Zhang, X., Wang, Y. & Pei, W. Implantable intracortical microelectrodes: reviewing the present with a focus on the future. *Microsyst. Nanoeng.* **9**, 7 (2023).
10. Oh, S. et al. Softening implantable bioelectronics: material designs, applications, and future directions. *Biosens. Bioelectron.* **258**, 116328 (2024).
11. Xu, M. et al. Nanorobots mediated drug delivery for brain cancer active targeting and controllable therapeutics. *Discov. Nano* **19**, 183 (2024).
12. Dijk, G., Ruigrok, H. J. & O'Connor, R. P. Influence of PEDOT:PSS coating thickness on the performance of stimulation electrodes. *Adv. Mater. Interfaces* **7**, 2000675 (2020).
13. Su, Z. et al. PEDOT:PSS and its composites for flexible supercapacitors. *ACS Appl. Energy Mater.* **5**, 11915–11932 (2022).
14. Yuk, H. et al. 3D printing of conducting polymers. *Nat. Commun.* **11**, 1604 (2020).
15. Puza, F. & Lienkamp, K. 3D printing of polymer hydrogels—from basic techniques to programmable actuation. *Adv. Funct. Mater.* **32**, 2205345 (2022).
16. Enrico, A. et al. Cleanroom-free direct laser micropatterning of polymers for organic electrochemical transistors in logic circuits and glucose biosensors. *Adv. Sci.* **11**, 2307042 (2024).
17. Polanía, R., Nitsche, M. A. & Ruff, C. C. Studying and modifying brain function with non-invasive brain stimulation. *Nat. Neurosci.* **21**, 174–187 (2018).
18. Scangos, K. W. et al. Closed-loop neuromodulation in an individual with treatment-resistant depression. *Nat. Med.* **27**, 1696–1700 (2021).
19. Lin, S. et al. Advanced electrode technologies for noninvasive brain–computer interfaces. *ACS Nano* **17**, 24487–24513 (2023).
20. Hsieh, J.-C. et al. A highly stable electrode with low electrode-skin impedance for wearable brain-computer interface. *Biosens. Bioelectron.* **218**, 114756 (2022).
21. Li, G. et al. Robust, self-adhesive, and low-contact impedance polyvinyl alcohol/polyacrylamide dual-network hydrogel semidry electrode for bio-potential signal acquisition. *SmartMat* **5**, e1173 (2024).
22. Qian, X. & Liao, C. Engineering liquid metal-based implantable electrodes toward brain-machine interfaces. *Health Sci. Rev.* **9**, 100118 (2023).
23. Jones, C. F., Resina, L., Ferreira, F. C., Sanjuan-Alberte, P. & Esteves, T. Conductive core–shell nanoparticles: synthesis and applications. *J. Phys. Chem. C.* **128**, 11083–11100 (2024).
24. Gueye, M. N., Carella, A., Faure-Vincent, J., Demadrille, R. & Simonato, J.-P. Progress in understanding structure and transport properties of PEDOT-based materials: a critical review. *Prog. Mater. Sci.* **108**, 100616 (2020).
25. Fan, X. et al. PEDOT:PSS for flexible and stretchable electronics: modifications, strategies, and applications. *Adv. Sci.* **6**, 1900813 (2019).
26. Kayser, L. V. & Lipomi, D. J. Stretchable conductive polymers and composites based on PEDOT and PEDOT:PSS. *Adv. Mater.* **31**, 1806133 (2019).
27. Rebetez, G., Bardagot, O., Affolter, J., Réhault, J. & Banerji, N. What drives the kinetics and doping level in the electrochemical reactions of PEDOT:PSS? *Adv. Funct. Mater.* **32**, 2105821 (2022).
28. Adilbekova, B. et al. Enhancing the electrical conductivity and long-term stability of PEDOT:PSS electrodes through sequential treatment with nitric acid and cesium chloride. *Adv. Mater.* **36**, 2405094 (2024).
29. Li, Y. et al. Boosting the performance of PEDOT:PSS based electronics via ionic liquids. *Adv. Mater.* **36**, 2310973 (2024).
30. Xing, W. et al. Omnidirectional printing of PEDOT:PSS for high-conductivity spanning structures. *ACS Appl. Mater. Interfaces* **15**, 57717–57725 (2023).
31. Li, W., Li, Y., Song, Z., Wang, Y.-X. & Hu, W. PEDOT-based stretchable optoelectronic materials and devices for bioelectronic interfaces. *Chem. Soc. Rev.* **53**, 10575–10603 (2024).
32. Won, D. et al. Digital selective transformation and patterning of highly conductive hydrogel bioelectronics by laser-induced phase separation. *Sci. Adv.* **8**, eabo3209 (2022).
33. Lo, L. W. et al. An inkjet-printed PEDOT:PSS-based stretchable conductor for wearable health monitoring device applications. *ACS Appl Mater. Interfaces* **13**, 21693–21702 (2021).
34. Liu, L. et al. Conductivity and stability enhancement of PEDOT:PSS electrodes via facile doping of sodium 3-methylsalicylate for highly efficient flexible organic light-emitting diodes. *ACS Appl Mater. Interfaces* **14**, 1615–1625 (2022).
35. Wei, Q., Mukaida, M., Naitoh, Y. & Ishida, T. Morphological change and mobility enhancement in PEDOT:PSS by adding co-solvents. *Adv. Mater.* **25**, 2831–2836 (2013).
36. Lingstedt, L. V. et al. Effect of DMSO solvent treatments on the performance of PEDOT:PSS based organic electrochemical transistors. *Adv. Electron. Mater.* **5**, 1800804 (2019).
37. Jeong, H. J., Jang, H., Kim, T., Earmme, T. & Kim, F. S. Sigmoidal dependence of electrical conductivity of thin PEDOT:PSS films on concentration of linear glycols as a processing additive. *Mater.* **14**, 1975 (2021).

38. Kato, M., Sano, H., Kiyobayashi, T., Takeichi, N. & Yao, M. Improvement of the battery performance of indigo, an organic electrode material, using PEDOT/PSS with D-sorbitol. *ACS Omega* **5**, 18565–18572 (2020).
39. Wu, M., Zhao, D., Wang, Z. & Yu, J. High-luminance perovskite light-emitting diodes with high-polarity alcohol solvent treating PEDOT:PSS as hole transport layer. *Nanoscale Res. Lett.* **13**, 128 (2018).
40. Rwei, S. P., Lee, Y. H., Shiu, J. W., Sasikumar, R. & Shyr, U. T. Characterization of solvent-treated PEDOT:PSS thin films with enhanced conductivities. *Polymers* **11**, 134 (2019).
41. Curreri, A. M., Mitragotri, S. & Tanner, E. E. L. Recent advances in ionic liquids in biomedicine. *Adv. Sci.* **8**, e2004819 (2021).
42. Tanner, E. E. L. Ionic liquids charge ahead. *Nat. Chem.* **14**, 842–842 (2022).
43. Li, Q. et al. Anion size effect of ionic liquids in tuning the thermoelectric and mechanical properties of PEDOT:PSS films through a counterion exchange strategy. *ACS Appl Mater. Interfaces* **14**, 27911–27921 (2022).
44. Feig, V. R., Tran, H., Lee, M. & Bao, Z. Mechanically tunable conductive interpenetrating network hydrogels that mimic the elastic moduli of biological tissue. *Nat. Commun.* **9**, 2740 (2018).
45. Oh, B. et al. 3D printable and biocompatible PEDOT:PSS-ionic liquid colloids with high conductivity for rapid on-demand fabrication of 3D bioelectronics. *Nat. Commun.* **15**, 5839 (2024).
46. Choi, C. et al. Hard-cation-soft-anion ionic liquids for PEDOT:PSS treatment. *J. Phys. Chem. B* **126**, 1615–1624 (2022).
47. Jiang, X. et al. Stretchable PEDOT:PSS/Li-TFSI/XSB composite films for electromagnetic interference shielding. *ACS Appl Mater. Interfaces* **15**, 8521–8529 (2023).
48. Lu, Y., Wu, A., Sha, C., Hang, X. C. & Young, D. J. Structural modulation induced by cobalt-based ionic liquids for enhanced thermoelectric transport in PEDOT:PSS. *Chem. Asian J.* **16**, 2740–2744 (2021).
49. Tang, C. G. et al. A universal biocompatible and multifunctional solid electrolyte in p-type and n-type organic electrochemical transistors for complementary circuits and bioelectronic interfaces. *Adv. Mater.* **36**, 2405556 (2024).
50. Li, T. et al. Biocompatible ionic liquids in high-performing organic electrochemical transistors for ion detection and electrophysiological monitoring. *ACS Nano* **16**, 12049–12060 (2022).
51. Tolmachev, D. et al. Computer simulations of deep eutectic solvents: challenges, solutions, and perspectives. *Int. J. Mol. Sci.* **23**, 645 (2022).
52. Aguzin, A. et al. Direct ink writing of PEDOT eutectogels as substrate-free dry electrodes for electromyography. *Mater. Horiz.* **10**, 2516–2524 (2023).
53. Wu, W. et al. Structural-induced effects of DES in PEDOT:PSS aqueous polymerization. *Polym. Test.* **129**, 108272 (2023).
54. Hansen, B. B. et al. Deep eutectic solvents: a review of fundamentals and applications. *Chem. Rev.* **121**, 1232–1285 (2021).
55. Ruiz-Mateos Serrano, R. et al. 3D printed PEDOT:PSS-based conducting and patternable eutectogel electrodes for machine learning on textiles. *Biomaterials* **310**, 122624 (2024).
56. Li, T. et al. Robust skin-integrated conductive biogel for high-fidelity detection under mechanical stress. *Nat. Commun.* **16**, 88 (2025).
57. Oh, J. Y., Kim, S., Baik, H.-K. & Jeong, U. Conducting polymer dough for deformable electronics. *Adv. Mater.* **28**, 4455–4461 (2016).
58. Chen, R. et al. PEDOT:PSS as stretchable conductors with good wettability on the substrate through the simultaneous plasticization and secondary doping with a cationic or anionic surfactant. *Macromolecules* **55**, 4967–4978 (2022).
59. Yoon, S.-S. & Khang, D.-Y. Roles of nonionic surfactant additives in PEDOT:PSS thin films. *J. Phys. Chem. C.* **120**, 29525–29532 (2016).
60. Vosgueritchian, M., Lipomi, D. J. & Bao, Z. Highly conductive and transparent PEDOT:PSS films with a fluorosurfactant for stretchable and flexible transparent electrodes. *Adv. Funct. Mater.* **22**, 421–428 (2012).
61. Zhang, S. et al. Solvent-induced changes in PEDOT:PSS films for organic electrochemical transistors. *APL Mater.* **3**, 014911 (2014).
62. Shrestha, M., Lu, Z. & Lau, G. K. Transparent tunable acoustic absorber membrane using inkjet-printed PEDOT:PSS thin-film compliant electrodes. *ACS Appl Mater. Interfaces* **10**, 39942–39951 (2018).
63. Ichikawa, S. & Toshima, N. Improvement of thermoelectric properties of composite films of PEDOT-PSS with xylitol by means of stretching and solvent treatment. *Polym. J.* **47**, 522–526 (2015).
64. Yao, B. et al. Ultrahigh-conductivity polymer hydrogels with arbitrary structures. *Adv. Mater.* https://doi.org/10.1002/adma.201700974 (2017).
65. Ouyang, J. Solution-processed PEDOT:PSS films with conductivities as indium tin oxide through a treatment with mild and weak organic acids. *ACS Appl Mater. Interfaces* **5**, 13082–13088 (2013).
66. Zhang, L. et al. The role of mineral acid doping of PEDOT:PSS and its application in organic photovoltaics. *Adv. Electron. Mater.* **6**, 1900648 (2020).
67. Chong, E. T. J., Ng, J. W. & Lee, P. -C. Classification and medical applications of biomaterials–a mini review. *BIO Integr.* https://doi.org/10.15212/bioi-2022-0009 (2023).
68. Wang, Y. et al. Engineering PEDOT:PSS/PEG fibers with a textured surface toward comprehensive personal thermal management. *ACS Appl Mater. Interfaces* **15**, 17175–17187 (2023).
69. Cao, J. et al. Stretchable and self-adhesive PEDOT:PSS blend with high sweat tolerance as conformal biopotential dry electrodes. *ACS Appl Mater. Interfaces* **14**, 39159–39171 (2022).
70. Sau, S. & Kundu, S. Fabrication of highly stretchable salt and solvent blended PEDOT:PSS/PVA free-standing films: non-linear to linear electrical conduction response. *RSC Adv.* **14**, 5193–5206 (2024).
71. Shi, W. et al. High-sensitivity and extreme environment-resistant sensors based on PEDOT:PSS@PVA hydrogel fibers for physiological monitoring. *ACS Appl Mater. Interfaces* **14**, 35114–35125 (2022).
72. Yu, J. et al. 3D printing of robust high-performance conducting polymer hydrogel-based electrical bioadhesive interface for soft bioelectronics. *Small* **20**, e2308778 (2024).
73. Almasri, R. M., AlChamaa, W., Tehrani-Bagha, A. R. & Khraiche, M. L. Highly flexible single-unit resolution all printed neural interface on a bioresorbable backbone. *ACS Appl Bio Mater.* **3**, 7040–7051 (2020).
74. Islam, G. M. N., Collie, S., Qasim, M. & Ali, M. A. Highly stretchable and flexible melt spun thermoplastic conductive yarns for smart textiles. *Nanomaterials* **10**, 2324 (2020).
75. Niu, Z. & Yuan, W. Smart nanocomposite nonwoven wearable fabrics embedding phase change materials for highly efficient energy conversion-storage and use as a stretchable conductor. *ACS Appl Mater. Interfaces* **13**, 4508–4518 (2021).
76. Cuttaz, E. et al. Conductive elastomer composites for fully polymeric, flexible bioelectronics. *Biomater. Sci.* **7**, 1372–1385 (2019).
77. Lee, J. H. et al. Highly conductive, stretchable, and transparent PEDOT:PSS electrodes fabricated with triblock copolymer additives and acid treatment. *ACS Appl Mater. Interfaces* **10**, 28027–28035 (2018).
78. Kim, J. et al. Hierarchically structured conductive polymer binders with silver nanowires for high-performance silicon anodes in lithium-ion batteries. *ACS Appl Mater. Interfaces* **14**, 17340–17347 (2022).
79. Kim, J. et al. Self-healing, stretchable and recyclable polyurethane-PEDOT:PSS conductive blends. *Mater. Horiz.* **11**, 3548–3560 (2024).
80. Verpoorten, E., Massaglia, G., Ciardelli, G., Pirri, C. F. & Quaglio, M. Design and optimization of piezoresistive PEO/PEDOT:PSS electrospun nanofibers for wearable flex sensors. *Nanomaterials* **10**, 2166 (2020).
81. McDonald, M. B. & Hammond, P. T. Efficient transport networks in a dual electron/lithium-conducting polymeric composite for electrochemical applications. *ACS Appl Mater. Interfaces* **10**, 15681–15690 (2018).
82. Plog, J., Wang, X., Lichade, K. M., Pan, Y. & Yarin, A. L. Extremely-fast electrostatically-assisted direct ink writing of 2D, 2.5D and 3D functional traces of conducting polymer Poly(3,4-ethylenedioxythiophene) polystyrene sulfonate- polyethylene oxide (PEDOT:PSS-PEO). *J. Colloid Interface Sci.* **651**, 1043–1053 (2023).
83. Zhou, J. & Hsieh, Y.-L. Conductive polymer protonated nanocellulose aerogels for tunable and linearly responsive strain sensors. *ACS Appl. Mater. Interfaces* **10**, 27902–27910 (2018).
84. Xu, X. & Hsieh, Y.-L. Aqueous exfoliated graphene by amphiphilic nanocellulose and its application in moisture-responsive foldable actuators. *Nanoscale* **11**, 11719–11729 (2019).
85. Jain, K., Reid, M. S., Larsson, P. A. & Wågberg, L. On the interaction between PEDOT:PSS and cellulose: adsorption mechanisms and controlling factors. *Carbohydr. Polym.* **260**, 117818 (2021).
86. Keshmiri, N. et al. Highly conductive polystyrene/carbon nanotube/PEDOT:PSS nanocomposite with segregated structure for electromagnetic interference shielding. *Carbon* **212**, 118104 (2023).
87. Pan, Y., He, M., Wu, J., Qi, H. & Cheng, Y. One-step synthesis of MXene-functionalized PEDOT:PSS conductive polymer hydrogels for wearable and noninvasive monitoring of sweat glucose. *Sens. Actuators B Chem.* **401**, 135055 (2024).

88. Wang, H. et al. Multifunctional filler-free PEDOT:PSS hydrogels with ultrahigh electrical conductivity induced by Lewis-acid-promoted ion exchange. *Adv. Mater.* **35**, e2302919 (2023).
89. Liu, J. et al. Additive manufacturing of Ti3C2-MXene-functionalized conductive polymer hydrogels for electromagnetic-interference shielding. *Adv. Mater.* **34**, 2106253 (2022).
90. Escudero, A. et al. Large-scale synthesis of hybrid conductive polymer-gold nanoparticles using "sacrificial" weakly binding ligands for printing electronics. *Inorg. Chem.* **60**, 17103–17113 (2021).
91. He, X. et al. Hexagonal and square patterned silver nanowires/PEDOT:PSS composite grids by screen printing for uniformly transparent heaters. *Polymers* **11**, 468 (2019).
92. Wei, Y. et al. Robust photodetectable paper from chemically exfoliated MoS(2)-MoO(3) multilayers. *ACS Appl Mater. Interfaces* **11**, 21445–21453 (2019).
93. Wang, B. et al. Carbon-based nanomaterials electrodes of ionic soft actuators: from initial 1D structure to 3D composite structure for flexible intelligent devices. *Small* **19**, 2304246 (2023).
94. Nenashev, G. V. et al. Effect of carbon dots concentration on electrical and optical properties of their composites with a conducting polymer. *Molecules* **27**, 8000 (2022).
95. Shao, Y. et al. Flexible pressure sensor with micro-structure arrays based on PDMS and PEDOT:PSS/PUD&CNTs composite film with 3D printing. *Materials* **14**, 6499 (2021).
96. Greco, G. et al. Pedot:PSS/graphene oxide (GO) ternary nanocomposites for electrochemical applications. *Molecules* **28**, 2963 (2023).
97. Khasim, S., Pasha, A., Badi, N., Lakshmi, M. & Mishra, Y. K. High performance flexible supercapacitors based on secondary doped PEDOT-PSS-graphene nanocomposite films for large area solid state devices. *RSC Adv.* **10**, 10526–10539 (2020).
98. Cao, J. et al. Self-healable PEDOT:PSS-PVA nanocomposite hydrogel strain sensor for human motion monitoring. *Nanomaterials* **13**, 2465 (2023).
99. Trivedi, S., Pamidi, V., Fichtner, M. & Reddy, M. A. Ionically conducting inorganic binders: a paradigm shift in electrochemical energy storage. *Green. Chem.* **24**, 5620–5631 (2022).
100. Reynolds, M. et al. Fabrication of sodium trimetaphosphate-based PEDOT:PSS conductive hydrogels. *Gels* **10**, 115 (2024).
101. Mydhili, V., Kavinkumar, T., Neppolian, B. & Manivannan, S. Electrochemical behaviour and temperature dependent electrical transitions in graphene oxide incorporated poly(vinyl alcohol)/poly(3,4-ethylenedioxythiophene): poly(styrenesulfonate) composites for dielectric and supercapacitor applications. *Mater. Chem. Phys.* **225**, 261–271 (2019).
102. Lakkala, P., Munnangi, S. R., Bandari, S. & Repka, M. Additive manufacturing technologies with emphasis on stereolithography 3D printing in pharmaceutical and medical applications: a review. *Int. J. Pharm. X* **5**, 100159 (2023).
103. Zakeri, S., Vippola, M. & Levänen, E. A comprehensive review of the photopolymerization of ceramic resins used in stereolithography. *Addit. Manuf.* **35**, 101177 (2020).
104. Zhou, L.-Y., Fu, J. & He, Y. A review of 3D printing technologies for soft polymer materials. *Adv. Funct. Mater.* **30**, 2000187 (2020).
105. Lopez-Larrea, N. et al. Digital light 3D printing of PEDOT-based photopolymerizable inks for biosensing. *ACS Appl. Polym. Mater.* **4**, 6749–6759 (2022).
106. Kong, T. F. et al. A newly crosslinked-double network PEDOT:PSS@PEGDMA toward highly-efficient and stable tin-lead perovskite solar cells. *Small* **19**, e2303159 (2023).
107. Lee, J. J. et al. The 3D printed conductive grooved topography hydrogel combined with electrical stimulation for synergistically enhancing wound healing of dermal fibroblast cells. *Biomater. Adv.* **142**, 213132 (2022).
108. Schaubroeck, D. et al. Surface analysis of the selective excimer laser patterning of a thin PEDOT:PSS film on flexible polymer films. *Appl. Surf. Sci.* **376**, 151–160 (2016).
109. Li, Y. et al. An injectable, self-healable, and reusable PEDOT:PSS/PVA hydrogel patch electrode for epidermal electronics. *Nano Res.* **17**, 5479–5490 (2024).
110. Liang, J. et al. MXene reinforced PAA/PEDOT:PSS/MXene conductive hydrogel for highly sensitive strain sensors. *Macromol. Mater. Eng.* **308**, 2200519 (2023).
111. Kim, N. et al. Elastic conducting polymer composites in thermoelectric modules. *Nat. Commun.* **11**, 1424 (2020).
112. Zhao, Y. et al. Ultra-conformal skin electrodes with synergistically enhanced conductivity for long-time and low-motion artifact epidermal electrophysiology. *Nat. Commun.* **12**, 4880 (2021).
113. Cheng, S., Zhu, R. & Xu, X. Hydrogels for next generation neural interfaces. *Commun. Mater.* **5**, 99 (2024).
114. Lunghi, A. et al. Flexible neural interfaces based on 3D PEDOT:PSS micropillar arrays. *Adv. Mater. Interfaces* **9**, 2200709 (2022).
115. Kim, S.-M. et al. Influence of PEDOT:PSS crystallinity and composition on electrochemical transistor performance and long-term stability. *Nat. Commun.* **9**, 3858 (2018).
116. Xu, S. & Wu, W. Ink-based additive nanomanufacturing of functional materials for human-integrated smart wearables. *Adv. Intell. Syst.* **2**, 2000117 (2020).
117. Gao, H. et al. 3D printed optics and photonics: processes, materials and applications. *Mater. Today* **69**, 107–132 (2023).
118. Wu, K. et al. Direct ink writing of PEDOT:PSS inks for flexible microsupercapacitors. *J. Ind. Eng. Chem.* **123**, 272–277 (2023).
119. Baniasadi, H. et al. Innovations in hydrogel-based manufacturing: a comprehensive review of direct ink writing technique for biomedical applications. *Adv. Colloid Interface Sci.* **324**, 103095 (2024).
120. Sanviti, M., Mester, L., Hillenbrand, R., Alegría, A. & Martínez-Tong, D. E. Solvent-structured PEDOT:PSS surfaces: fabrication strategies and nanoscale properties. *Polymer* **246**, 124723 (2022).
121. Lu, B. et al. Pure PEDOT:PSS hydrogels. *Nat. Commun.* **10**, 1043 (2019).
122. Zeng, L. et al. Direct ink writing 3D printing for high-performance electrochemical energy storage devices: a minireview. *Adv. Sci.* **10**, 2303716 (2023).
123. Hill, I. M. et al. Imparting high conductivity to 3D printed PEDOT:PSS. *ACS Appl. Polym. Mater.* **5**, 3989–3998 (2023).
124. Yang, J., He, P. & Derby, B. Stability bounds for micron scale Ag conductor lines produced by electrohydrodynamic inkjet printing. *ACS Appl. Mater. Interfaces* **14**, 39601–39609 (2022).
125. Carou-Senra, P. et al. Inkjet printing of pharmaceuticals. *Adv. Mater.* **36**, e2309164 (2024).
126. Otowa, T., Tsubouchi, S. & Suwa, Y. Analysis of the ink-stream break-up phenomenon in continuous inkjet printing. *ACS Omega* **8**, 34442–34447 (2023).
127. Cao, T., Yang, Z., Zhang, H. & Wang, Y. Inkjet printing quality improvement research progress: a review. *Heliyon* **10**, e30163 (2024).
128. Qian, Q. et al. 3D reactive inkjet printing of bisphenol A-polycarbonate. *Addit. Manuf.* **54**, 102745 (2022).
129. Wijshoff, H. Drop dynamics in the inkjet printing process. *Curr. Opin. Colloid Interface Sci.* **36**, 20–27 (2018).
130. Ruggiero, A. et al. Two-photon polymerization lithography enabling the fabrication of PEDOT:PSS 3D structures for bioelectronic applications. *Chem. Commun.* **58**, 9790–9793 (2022).
131. Lu, G., Tang, R., Nie, J. & Zhu, X. Photocuring 3D printing of hydrogels: techniques, materials, and applications in tissue engineering and flexible devices. *Macromol. Rapid Commun.* **45**, 2300661 (2024).
132. Bertana, V. et al. Rapid prototyping of 3D organic electrochemical transistors by composite photocurable resin. *Sci. Rep.* **10**, 13335 (2020).
133. Agresti, A., Di Giacomo, F., Pescetelli, S. & Di Carlo, A. Scalable deposition techniques for large-area perovskite photovoltaic technology: a multiperspective review. *Nano Energy* **122**, 109317 (2024).
134. How, Y. Y. et al. A review on the binder-free electrode fabrication for electrochemical energy storage devices. *J. Energy Storage* **51**, 104324 (2022).
135. Ji, B. et al. Flexible bioelectrodes with enhanced wrinkle microstructures for reliable electrochemical modification and neuromodulation in vivo. *Biosens. Bioelectron.* **135**, 181–191 (2019).
136. Chen, J. V., Tanaka, K. S., Dang, A. B. C. & Dang, A. Identifying a commercially-available 3D printing process that minimizes model distortion after annealing and autoclaving and the effect of steam sterilization on mechanical strength. *3D Print. Med.* **6**, 9 (2020).
137. Carter, J. L., Kelly, C. A. & Jenkins, M. J. Processing optimization of PEDOT:PSS and PEDOT:PSS/Tween 80 films. *Polym. J.* **55**, 253–260 (2023).
138. Wang, Y. et al. Enhanced neural activity detection with microelectrode arrays modified by drug-loaded calcium alginate/chitosan hydrogel. *Biosens. Bioelectron.* **267**, 116837 (2025).
139. Ahmadi, N., Constandinou, T. G. & Bouganis, C.-S. Inferring entire spiking activity from local field potentials. *Sci. Rep.* **11**, 19045 (2021).
140. Engel, A. K., Moll, C. K. E., Fried, I. & Ojemann, G. A. Invasive recordings from the human brain: clinical insights and beyond. *Nat. Rev. Neurosci.* **6**, 35–47 (2005).

141. Nguyen, J.-P., Nizard, J., Keravel, Y. & Lefaucheur, J.-P. Invasive brain stimulation for the treatment of neuropathic pain. *Nat. Rev. Neurol.* **7**, 699–709 (2011).
142. Pei, F. & Tian, B. Nanoelectronics for minimally invasive cellular recordings. *Adv. Funct. Mater.* **30**, 1906210 (2020).
143. Wu, N. et al. Electrode materials for brain–machine interface: a review. *InfoMat* **3**, 1174–1194 (2021).
144. Ajmal Mokhtar, S. M. et al. Electrochemical stability of PEDOT for wearable on-skin application. *J. Appl. Polym. Sci.* **138**, 51314 (2021).
145. Long, M. A. & Lee, A. K. Intracellular recording in behaving animals. *Curr. Opin. Neurobiol.* **22**, 34–44 (2012).
146. Kubska, Z. R. & Kamiński, J. How human single-neuron recordings can help us understand cognition: insights from memory studies. *Brain Sci.* **11**, 443 (2021).
147. Lee, A. K. & Brecht, M. Elucidating neuronal mechanisms using intracellular recordings during behavior. *Trends Neurosci.* **41**, 385–403 (2018).
148. Chung, J. E. et al. High-density single-unit human cortical recordings using the neuropixels probe. *Neuron* **110**, 2409–2421.e2403 (2022).
149. Lempka, S. F. et al. Optimization of microelectrode design for cortical recording based on thermal noise considerations. In *2006 International Conference of the IEEE Engineering in Medicine and Biology Society* 3361–3364 (IEEE, 2006).
150. Lewis, C. M. et al. Recording quality is systematically related to electrode impedance. *Adv. Healthc. Mater.* **13**, 2303401 (2024).
151. Du, Z. J., Luo, X., Weaver, C. L. & Cui, X. T. Poly(3,4-ethylenedioxythiophene)-ionic liquid coating improves neural recording and stimulation functionality of MEAs. *J. Mater. Chem. C.* **3**, 6515–6524 (2015).
152. Zeng, M. et al. Dopamine-integrated all-hydrogel multi-electrode arrays for neural activity recording. *Mater. Horiz.* **11**, 6423–6434 (2024).
153. Sinha, M. & Narayanan, R. Active dendrites and local field potentials: biophysical mechanisms and computational explorations. *Neuroscience* **489**, 111–142 (2022).
154. Li, M. et al. Brain–computer interface for simultaneous dual-region spatial coding in hippocampal and somatosensory cortex of freely behaving rats. *Electron. Lett.* **60**, e70013 (2024).
155. Yan, M. et al. Conducting polymer-hydrogel interpenetrating networks for improving the electrode–neural interface. *ACS Appl. Mater. Interfaces* **15**, 41310–41323 (2023).
156. Yang, J. C. et al. Microscale dynamics of electrophysiological markers of epilepsy. *Clin. Neurophysiol.* **132**, 2916–2931 (2021).
157. Han, M. et al. Utilizing GO/PEDOT:PSS/PtNPs-enhanced high-stability microelectrode arrays for investigating epilepsy-induced striatal electrophysiology alterations. *Front. Bioeng. Biotechnol.* **12**, 1376151 (2024).
158. Jing, L. et al. Deep brain implantable microelectrode arrays for detection and functional localization of the subthalamic nucleus in rats with Parkinson's disease. *Bio-Des. Manuf.* **7**, 439–452 (2024).
159. Lu, Z. et al. PtNPt/MWCNT-PEDOT:PSS-modified microelectrode arrays for the synchronous dopamine and neural spike detection in rat models of sleep deprivation. *ACS Appl. Bio Mater.* **4**, 4872–4884 (2021).
160. Lee, J., Ozden, I., Song, Y.-K. & Nurmikko, A. V. Transparent intracortical microprobe array for simultaneous spatiotemporal optical stimulation and multichannel electrical recording. *Nat. Methods* **12**, 1157–1162 (2015).
161. Li, H., Wang, J. & Fang, Y. Recent developments in multifunctional neural probes for simultaneous neural recording and modulation. *Microsyst. Nanoeng.* **9**, 4 (2023).
162. Ganji, M., Tanaka, A., Gilja, V., Halgren, E. & Dayeh, S. A. Scaling effects on the electrochemical stimulation performance of Au, Pt, and PEDOT:PSS electrocorticography arrays. *Adv. Funct. Mater.* **27**, 1703019 (2017).
163. Ersöz, A., Kim, I. & Han, M. Maximizing charge injection limits of iridium oxide electrodes with a programmable anodic bias circuit. *Int. IEEE EMBS Conf. Neural Eng.* **2021**, 540–543 (2021).
164. Wang, X. et al. Ultraflexible PEDOT:PSS/IrO(x)-modified electrodes: applications in behavioral modulation and neural signal recording in mice. *Micromachines* **15**, 447 (2024).
165. Chik, G. K. K. et al. Flexible multichannel neural probe developed by electropolymerization for localized stimulation and sensing. *Adv. Mater. Technol.* **7**, 2200143 (2022).
166. Uguz, I. & Shepard, K. L. Spatially controlled, bipolar, cortical stimulation with high-capacitance, mechanically flexible subdural surface microelectrode arrays. *Sci. Adv.* **8**, eabq6354 (2022).
167. Liu, C. et al. A wireless, implantable optoelectrochemical probe for optogenetic stimulation and dopamine detection. *Microsyst. Nanoeng.* **6**, 64 (2020).
168. Moon, H. et al. Electrocorticogram (ECoG): engineering approaches and clinical challenges for translational medicine. *Adv. Mater. Technol.* **9**, 2301692 (2024).
169. Wei, S. et al. Shape-changing electrode array for minimally invasive large-scale intracranial brain activity mapping. *Nat. Commun.* **15**, 715 (2024).
170. Yang, W., Gong, Y. & Li, W. A review: electrode and packaging materials for neurophysiology recording implants. *Front. Bioeng. Biotechnol.* **8**, 622923 (2020).
171. Ganji, M. et al. Development and translation of PEDOT:PSS microelectrodes for intraoperative monitoring. *Adv. Funct. Mater.* **28**, 1700232 (2018).
172. Li, X. et al. PDMS–parylene hybrid, flexible micro-ECoG electrode array for spatiotemporal mapping of epileptic electrophysiological activity from multicortical brain regions. *ACS Appl. Bio Mater.* **4**, 8013–8022 (2021).
173. Donahue, M. J. et al. Multimodal characterization of neural networks using highly transparent electrode arrays. *eneuro* **5**, ENEURO.0187-0118.2018 (2018).
174. Blau, R. et al. Surface-grafted biocompatible polymer conductors for stable and compliant electrodes for brain interfaces. *Adv. Healthc. Mater.* **13**, e2402215 (2024).
175. Spyropoulos, G. D. et al. Transcranial electrical stimulation and recording of brain activity using freestanding plant-based conducting polymer hydrogel composites. *Adv. Mater. Technol.* **5**, 1900652 (2020).
176. Cho, Y. U., Lim, S. L., Hong, J.-H. & Yu, K. J. Transparent neural implantable devices: a comprehensive review of challenges and progress. *npj Flex. Electron.* **6**, 53 (2022).
177. Zheng, Y. et al. Coagulation bath-assisted 3D printing of PEDOT:PSS with high resolution and strong substrate adhesion for bioelectronic devices. *Adv. Mater. Technol.* **7**, 2101514 (2022).
178. Cui, Y. et al. A stretchable and transparent electrode based on PEGylated silk fibroin for in vivo dual-modal neural-vascular activity probing. *Adv. Mater.* **33**, 2100221 (2021).
179. Cho, Y. U. et al. MRI-compatible, transparent PEDOT:PSS neural implants for the alleviation of neuropathic pain with motor cortex stimulation. *Adv. Funct. Mater.* **34**, 2310908 (2024).
180. López-Alonso, V., Cheeran, B., Río-Rodríguez, D. & Fernández-del-Olmo, M. Inter-individual variability in response to non-invasive brain stimulation paradigms. *Brain Stimul.* **7**, 372–380 (2014).
181. Li, Y. et al. Advancing EEG-based brain-computer interface technology via PEDOT:PSS electrodes. *Matter* **7**, 2859–2895 (2024).
182. Biasiucci, A., Franceschiello, B. & Murray, M. M. Electroencephalography. *Curr. Biol.* **29**, R80–R85 (2019).
183. Górecka, J. & Makiewicz, P. The dependence of electrode impedance on the number of performed EEG examinations. *Sensors* **19**, 2608 (2019).
184. Zhao, Y. et al. Ultra-conductive and transparent epidermal electrodes for simultaneous dual-mode assessment of brain function. *Chem. Eng. J.* **476**, 146628 (2023).
185. Liu, J. et al. Ten-hour stable noninvasive brain-computer interface realized by semidry hydrogel-based electrodes. *Research* **2022**, 9830457 (2022).
186. Saha, S. et al. Progress in brain computer interface: challenges and opportunities. *Front. Syst. Neurosci.* **15**, 578875 (2021).
187. Hinrichs, H. et al. Comparison between a wireless dry electrode EEG system with a conventional wired wet electrode EEG system for clinical applications. *Sci. Rep.* **10**, 5218 (2020).
188. Yang, L. et al. Materials for dry electrodes for the electroencephalography: advances, challenges, perspectives. *Adv. Mater. Technol.* **7**, 2100612 (2022).
189. Xue, H. et al. Hydrogel electrodes with conductive and substrate-adhesive layers for noninvasive long-term EEG acquisition. *Microsyst. Nanoeng.* **9**, 79 (2023).
190. Seiti, M., Giuri, A., Corcione, C. E. & Ferraris, E. Advancements in tailoring PEDOT: PSS properties for bioelectronic applications: a comprehensive review. *Biomater. Adv.* **154**, 213655 (2023).
191. Jorge, S. M., Santos, L. F., Galvão, A., Morgado, J. & Charas, A. Concurrent enhancement of conductivity and stability in water of poly(3,4-Ethylenedioxythiophene):poly(Styrenesulfonate) films using an oxetane additive. *Adv. Mater. Interfaces* **8**, 2100517 (2021).
192. Kim, S.-M. et al. High-performance, polymer-based direct cellular interfaces for electrical stimulation and recording. *NPG Asia Mater.* **10**, 255–265 (2018).
193. Singh, A., Katiyar, M. & Garg, A. Understanding the formation of PEDOT:PSS films by ink-jet printing for organic solar cell applications. *RSC Adv.* **5**, 78677–78685 (2015).
194. Carter, J. L., Kelly, C. A. & Jenkins, M. J. Enhanced adhesion of PEDOT:PSS to substrates using polydopamine as a primer. *Polym. J.* **56**, 115–120 (2024).

195. Fang, Y. et al. PEDOT: PSS-based microfluidic-spun microfibers for tunable release of acetaminophen via electrical stimulation. *Adv. Mater. Technol.* **7**, 2200103 (2022).
196. Zrenner, C. & Ziemann, U. Closed-loop brain stimulation. *Biol. Psychiatry* **95**, 545–552 (2024).
197. Uguz, I. et al. Autoclave sterilization of PEDOT:PSS electrophysiology devices. *Adv. Healthc. Mater.* **5**, 3094–3098 (2016).
198. Castagnola, E. et al. pHEMA encapsulated PEDOT-PSS-CNT microsphere microelectrodes for recording single unit activity in the brain. *Front. Neurosci.* **10**, 151 (2016).
199. Schander, A., Stemmann, H., Kreiter, A. K. & Lang, W. Silicon-based microfabrication of free-floating neural probes and insertion tool for chronic applications. *Micromachines* **9**, 131 (2018).
200. Filho, G. et al. All-polymeric electrode based on PEDOT:PSS for in vivo neural recording. *Biosensors* **12**, 853 (2022).
201. Wang, Y. et al. PtNPs/short MWCNT-PEDOT: PSS-modified microelectrode array to detect neuronal firing patterns in the dorsal raphe nucleus and hippocampus of insomnia rats. *Micromachines* **13**, 488 (2022).
202. Yang, G. C. et al. PtNPs/PEDOT:PSS-modified microelectrode arrays for detection of the discharge of head direction cells in the retrosplenial cortex of rats under dissociation between visual and vestibular inputs. *Biosensors* **13**, 496 (2023).
203. Schander, A. et al. Design and fabrication of novel multi-channel floating neural probes for intracortical chronic recording. *Sens. Actuators A Phys.* **247**, 125–135 (2016).
204. He, E. et al. SWCNTs/PEDOT:PSS-modified microelectrode arrays for dual-mode detection of electrophysiological signals and dopamine concentration in the striatum under isoflurane anesthesia. *ACS Sens.* **6**, 3377–3386 (2021).
205. Hong, J.-H. et al. Monolayer, open-mesh, pristine PEDOT:PSS-based conformal brain implants for fully MRI-compatible neural interfaces. *Biosens. Bioelectron.* **260**, 116446 (2024).
206. Wang, X. Y. et al. Ultraflexible PEDOT:PSS/IrOx-modified electrodes: applications in behavioral modulation and neural signal recording in mice. *Micromachines* **15**, 447 (2024).
207. Sun, S. K. et al. Nucleobase-modified adhesive and conductive hydrogel interface for bioelectronics. *Acs Appl. Nano Mater.* **6**, 21226–21235 (2023).
208. Vomero, M. et al. Glassy carbon electrocorticography electrodes on ultra-thin and finger-like polyimide substrate: performance evaluation based on different electrode diameters. *Materials* **11**, 2486 (2018).
209. Koschinski, L. et al. Validation of transparent and flexible neural implants for simultaneous electrophysiology, functional imaging, and optogenetics. *J. Mater. Chem. B* **11**, 9639–9657 (2023).
210. Tseghai, G. B., Malengier, B., Fante, K. A. & Van Langenhove, L. Dry electroencephalography textrode for brain activity monitoring. *IEEE Sens. J.* **21**, 22077–22085 (2021).
211. Xu, T. C. Well-modulated interfacial ion transport enables d-sorbitol/PEDOT:PSS fibers to sense brain electrophysiological signals in vivo. *Chem. Commun.* **60**, 8244–8247 (2024).